

SEARCH FOR DECAY MODES OF Ω^- IN $\psi(2S)$ DATA

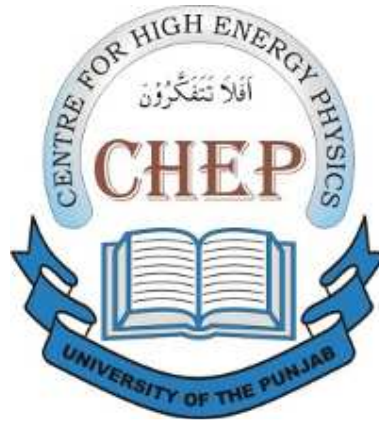


TALAB HUSSAIN

**Centre for High Energy Physics
University of the Punjab
Lahore-54590, Pakistan**

(February, 2010)

SEARCH FOR DECAY MODES OF Ω^- IN $\psi(2S)$ DATA



by

TALAB HUSSAIN

Submitted in Partial Fulfillment of the Requirements for the
Degree of DOCTOR OF PHILOSOPHY

at

**Centre for High Energy Physics
University of the Punjab
Lahore-54590, Pakistan**

(February, 2010)

**SEARCH FOR DECAY MODES OF Ω^-
IN $\psi(2S)$ DATA**

by

TALAB HUSSAIN

Submitted in Partial Fulfillment of the Requirements
for the Degree of DOCTOR OF PHILOSOPHY

Centre for High Energy Physics

University of the Punjab

Lahore-54590, Pakistan

February, 2010

DEDICATED
TO
MY PARENTS, FAMILY AND TEACHERS

CERTIFICATE

It is certified that I have read this dissertation and that, in my opinion, it is fully adequate in scope and quality for the degree of Doctor of Philosophy.

Prof. Shan Jin
(Supervisor)

Prof. Dr. Haris Rashid
(Supervisor)

Submitted through

Prof. Dr. Haris Rashid
(Supervisor & Director)

DECLARATION

Physics results reported in this thesis were determined using 14 million $\psi(2S)$ events recorded at Beijing Spectrometer II (BESII) experiment. Initially, the results were presented in physics meetings of Charmonium Group at Institute of High Energy Physics, Beijing, China. Details were further scrutinized by three referees of BES Collaboration. After the referees agreed, a draft paper titled *First Evidence of $\psi(2S) \rightarrow \Omega^-\bar{\Omega}^+$* , was submitted to the Collaboration.

This thesis is being submitted to the University of the Punjab, to meet the partial requirements of the DEGREE OF PHILOSOPHY in the field of 'Experimental High Energy Physics'. It does not contain any material already submitted for any degree or diploma in any university. To the best of my knowledge, there is no material published or written by another person, except with references. If any reference is found missing, that would be completely unintentional and I do not pretend to own any credit for that.

Talab Hussain

ACKNOWLEDGEMENTS

In the name of Almighty Allah, Who blessed me with strength and devotion in completing this challenging task. I have no words to thank my supervisors: Prof. Dr. Haris Rashid and Prof. Shan Jin for their kind and encouraging guidance towards achieving this goal. I would like to thank the IHEP authorities, for providing me excellent opportunity to perform research work using BESII experimental data. A lot of thanks to the BES collaboration for a disciplined way of scrutinizing my physics results. I am deeply thankful to the BES referees: Chengping, Wang Zhiyong and Xiaoling, for making me improve my research details. I would like to thank all those who encouraged me throughout my research period at IHEP. Bundle of thanks to Jia Yinghua and Shoupin Wen who helped me a lot during my stay at IHEP.

I am really thankful to Higher Education Commision (HEC), Islamabad, Pakistan, for providing financial support to complete this work effectively. Thanks to Dr. Qadeer Afzal Malik, Abrar Ahmed zafar, Tariq Mahmood and Muhammad Anjum Javed for their moral support throughout the research period.

I am thankful to my parents whose prayers made it possible to attain this goal. Last but not the *least*, I am deeply indebted to patient and encouraging role of my wife and loving children during this entire period of my doctoral studies.

Talab Hussain

THE AUTHOR

Name: Talab Hussain

Qualifications:

- MSc (High Energy Physics)
- MSc (Computer Science)
- MPhil (High Energy Physics)

Publications:

1. A draft paper titled *First Evidence of $\psi(2S) \rightarrow \Omega^- \bar{\Omega}^+$* , submitted to the BES Collaboration.
2. *GEANT4: Applications in High Energy Physics*, AIP Conf. Proc. – February 14, 2007 – Volume 888, pp. 301-304.

TABLE OF CONTENTS

ABSTRACT	XI
LIST OF FIGURES	XII
LIST OF TABLES	XVII
1 INTRODUCTION	1
2 PARTICLES AND THEIR INTERACTIONS	4
2.1 Fundamental Particles	4
2.2 Fundamental Interactions	6
2.3 Mesons	9
2.4 Baryons	12
2.4.1 Discovery of Ω^- and its Physical Significance	14
3 EXPERIMENTAL SETUP	16
3.1 Beijing Electron Positron Collider	16
3.2 BESII Detector	19

3.2.1	Beam Pipe	20
3.2.2	Vertex Chamber	20
3.2.3	Main Drift Chamber	21
3.2.4	Time-of-Flight (TOF) System	22
3.2.5	Electromagnetic Shower Counter	23
3.2.6	Muon Counter	24
3.3	Luminosity Measurements	24
3.4	Detector Background	25
3.5	Detector Performance	25
4	LITERATURE REVIEW	26
4.1	Electron Positron Collisions	26
4.1.1	Hadron Production	27
4.2	Charmonium States	29
4.2.1	Electromagnetic Transitions	32
4.2.2	Hadronic Transitions	32
4.2.3	Annihilation Decays	33
4.3	Non-Leptonic Decays of Ω^- and $\bar{\Omega}^+$	36
4.4	Search for Ω^- and $\bar{\Omega}^+$ in $\psi(2S)$ Decays	39
5	STUDY OF $\psi(2S) \rightarrow \Omega^- \bar{\Omega}^+$	42
5.1	Introduction	42
5.2	Monte-Carlo And Data Samples	43
5.3	Initial Event Selection	44

5.4	Particle Identification	45
5.5	Kinematic Fitting	47
5.6	Determination of $\Lambda(\bar{\Lambda})$ and $\Omega^-(\bar{\Omega}^+)$ Mass Resolutions	54
5.7	Optimization of χ_{1C}^2	54
5.8	Final Event Selection	55
5.9	Background Analysis	61
5.10	Statistical Significance of Ω^- and $\bar{\Omega}^+$ Signals	62
5.11	Detection Efficiency	63
5.12	Determination of Branching Fraction	64
5.13	Systematic Error Analysis	71
5.13.1	Models of Hadron Interaction	72
5.13.2	Particle Identification	72
5.13.3	MDC Tracking	73
5.13.4	4C Kinematic Fit	73
5.13.5	1C Kinematic Fit	73
5.13.6	Angular Distribution of Events	74
5.13.7	Monte Carlo Statistics	74
5.13.8	Intermediate Branching Fractions	75
5.13.9	Total Number of $\psi(2S)$ Data Events	76
6	DISCUSSION AND CONCLUSIONS	78
6.1	CONCLUSIONS	81

ABSTRACT

A detailed analysis of $\psi(2S) \rightarrow \Omega^-\bar{\Omega}^+$ ($\Omega^- \rightarrow \Lambda K^-$, $\Lambda \rightarrow p\pi^-$, $\bar{\Omega}^+ \rightarrow \bar{\Lambda}K^+$ and $\bar{\Lambda} \rightarrow \bar{p}\pi^+$) decay channel has been undertaken in this work. About 14 million $\psi(2S)$ decays recorded by Beijing Spectrometer II (BESII) at Beijing Electron Positron Collider (BEPC), have been used. In earlier measurements of $\psi(2S) \rightarrow \Omega^-\bar{\Omega}^+$, no significant signal of Ω^- or $\bar{\Omega}^+$ was found. Through a new technique of selecting events with one missing charge track also, we report a first evidence of Ω^- and $\bar{\Omega}^+$ signals with statistical significance levels of 5.3σ and 4.6σ , respectively. A branching fraction of $\psi(2S) \rightarrow \Omega^-\bar{\Omega}^+$ has been determined to be $(3.21 \pm 1.25 \pm 0.97) \times 10^{-5}$. The errors are statistical and systematic, respectively.

List of Figures

2.1	SU(4) meson multiplets made of up, down, strange and charm quark flavors. (a) SU(4) 16-plet for pseudoscalar mesons and (b) SU(4) 16-plet for vector mesons. The nonets of pseudoscalar and vector light mesons make the central planes. These planes also contain $c\bar{c}$ states [31].	10
2.2	SU(4) baryon multiplets made of up, down, strange and charm quarks. (a) The 20-plet with an SU(3) baryon octet. (b) The 20-plet with an SU(3) baryon decuplet [31].	13
3.1	Schematic diagram of Beijing Electron Positron Collider [37]	17
3.2	Side and end views of BESII detector ([38], [39]).	19
3.3	dE/dx (left) and TOF (right) resolutions at BESII [38], [39]	22
4.1	Ratio R as a function of center of mass energy \sqrt{s} , in the charmonium mass region ([38], [49]).	29
4.2	Known charmonium states and their radiative transitions: electromagnetic and hadronic. The dotted lines indicate threshold energy levels for charmonium decays into pairs of charmed mesons [50].	31

4.3	Electromagnetic decays of ψ family [61]	33
4.4	The XYZs of charmonium at BES [62]	34
4.5	Charmonium annihilation decay through three gluons and one photon [38]	35
4.6	Feynman diagrams for charmonium annihilation decays: (a) strong annihilation decay to baryon antibaryon pair (b) electromagnetic an- nihilation decay to baryon anti-baryon pair [67].	35
4.7	The left diagram (Tree-level diagram) represents change of strange quark flavor into an up quark flavor and the diagram on the right (Penguin diagram) shows how a strange quark flavor is changed into a down quark flavor [76]	38
4.8	BES Result: $Br(\psi(2S) \rightarrow \Omega^-\bar{\Omega}^+) \leq 7.3 \times 10^{-5}$ at 90% confidence level. The crosses represent the MC invariant mass distribution of ΛK^- normalized to the data events. Within 3σ signal region there are no data signal events [73].	40
4.9	CLEO Result: $Br(\psi(2S) \rightarrow \Omega^-\bar{\Omega}^+) \leq 1.6 \times 10^{-4}$ at 90% confidence level. Here, the invariant mass distribution of ΛK^- is only from data events [75].	41

5.1	The χ^2 distributions [82]: (a) χ^2_{4C} distribution: the histogram is for MC and the dots with error bars represent data events passing successfully through 4C kinematic fit (b) χ^2_{1C} distribution: the histogram is for MC and the dots with error bars represent data events obtained after 1C kinematic fit.	47
5.2	Momentum distributions (GeV/c) of final state particles: (a) proton (p) (b) antiproton (\bar{p}) (c) kaon (K^+) (d) kaon (k^-) (e) pion (π^+) and pion (π^-), of MC signal events passing successfully 4C or 1C kinematic fits, without any mass or χ^2 constraints [83].	49
5.3	Invariant mass spectra of $p\pi^-$ (GeV/ c^2) reconstructed by using four momenta of proton (p) and pion (π^-) belonging to the events passing 4C or 1C kinematic fit: (a) $M(p\pi^-)$ for MC events and (b) $M(p\pi^-)$ for data events, without any mass or χ^2 constraints [83].	50
5.4	$\bar{p}\pi^+$ invariant mass spectra (GeV/ c^2)reconstructed from four momenta of antiproton (\bar{p}) and pion (π^+) belonging to the events obtained from 4C or 1C kinematic fit: (a) from signal MC and (b) from data , without any mass or χ^2 constraints [83].	51
5.5	ΛK^- invariant mass spectra (GeV/ c^2) obtained by using four momenta of reconstructed Λ and K^- for events passing 4C or 1C kinematic fit: (a) from signal MC and (b) from data, without any mass or χ^2 constraints [83].	52

5.6	$\bar{\Lambda}K^+$ invariant mass spectra (GeV/c^2) obtained by using four momenta of reconstructed $\bar{\Lambda}$ and K^+ for events passing 4C or 1C kinematic fit: (a) from signal MC and (b) from data, without any mass or χ^2 constraints [83].	53
5.7	Optimization of χ_{1C}^2 : S represents the signal events whereas S+B represents signal plus background events. That χ_{1C}^2 cut is decided which optimizes the ratio: $S/\sqrt{S+B}$. In this way, the optimized cut is chosen to be $\chi_{1C}^2 < 10$ [83].	55
5.8	$p\pi^-$ invariant mass distributions: (a) from signal MC and (b) from data, under the constraints: $ M_{p\pi^+} - M_{\bar{\Lambda}} < 0.012 \text{ GeV}/c^2$ and ($\chi_{4C}^2 < 20$ or $\chi_{1C}^2 < 10$) [83].	57
5.9	$\bar{p}\pi^+$ invariant mass plots: (a) from signal MC and (b) from data, under the constraints: $ M_{p\pi^-} - M_{\Lambda} < 0.012 \text{ GeV}/c^2$ and ($\chi_{4C}^2 < 20$ or $\chi_{1C}^2 < 10$) [83].	58
5.10	ΛK^- invariant mass spectra: (a) from signal MC and (b) from data, under the constraints: $ M_{p\pi^-} - M_{\Lambda} < 0.012 \text{ GeV}/c^2$, $ M_{\bar{p}\pi^+} - M_{\bar{\Lambda}} < 0.012 \text{ GeV}/c^2$, $ M_{\bar{\Lambda}K^+} - M_{\bar{\Omega}^+} < 0.025 \text{ GeV}/c^2$ and ($\chi_{4C}^2 < 20$ or $\chi_{1C}^2 < 10$)[83].	59
5.11	$\bar{\Lambda}K^+$ invariant mass distributions: (a) from signal MC and (b) from data, under the constraints: $ M_{p\pi^-} - M_{\Lambda} < 0.012 \text{ GeV}/c^2$, $ M_{\bar{p}\pi^+} - M_{\bar{\Lambda}} < 0.012 \text{ GeV}/c^2$, $ M_{\Lambda K^-} - M_{\Omega^-} < 0.025 \text{ GeV}/c^2$ and ($\chi_{4C}^2 < 20$ or $\chi_{1C}^2 < 10$) [83].	60

- 5.12 Scatter Plot of $\bar{\Lambda}K^+$ versus ΛK^- for data events, under the constraints:
 $|M_{p\pi^-} - M_\Lambda| < 0.012 \text{ GeV}/c^2$, $|M_{\bar{p}\pi^+} - M_{\bar{\Lambda}}| < 0.012 \text{ GeV}/c^2$ and
 $\chi_{4C}^2 < 20$ (for those events which are obtained through 4C kinematic
fit) or $\chi_{1C}^2 < 10$ (for events obtained via 1C kinematic fit) [83]. 61
- 5.13 Fit to ΛK^- invariant mass spectrum, using signal MC histogram of
 ΛK^- invariant mass spectrum as signal shape and histogram of ΛK^-
invariant mass spectrum from $\psi(2S) \rightarrow \Lambda \bar{\Lambda} K^+ K^-$ as phase space back-
ground shape. The squares with error bars represent data. Background
in the signal region is negligible as shown in the figure ([82], [83]). . . 66
- 5.14 Fit to ΛK^- invariant mass spectrum using only histogram of ΛK^-
invariant mass spectrum from $\psi(2S) \rightarrow \Lambda \bar{\Lambda} K^+ K^-$ as phase space
background shape (assuming no signal). The squares with error bars
represent data ([82], [83]). 67
- 5.15 Fit to $\bar{\Lambda}K^+$ invariant mass spectrum, using signal MC histogram of
 $\bar{\Lambda}K^+$ invariant mass spectrum as signal shape and histogram of $\bar{\Lambda}K^+$
invariant mass spectrum from $\psi(2S) \rightarrow \Lambda \bar{\Lambda} K^+ K^-$ as phase space back-
ground shape. The squares with error bars represent data. Background
in the signal region is not so large as shown in the figure ([82], [83]). . 68
- 5.16 Fit to $\bar{\Lambda}K^+$ invariant mass spectrum using only histogram of $\bar{\Lambda}K^+$
invariant mass spectrum from $\psi(2S) \rightarrow \Lambda \bar{\Lambda} K^+ K^-$ as phase space
background shape (assuming no signal). The squares with error bars
represent data ([82], [83]). 69

List of Tables

2.1	Additive quantum numbers of leptons [30, 32]	6
2.2	Additive quantum numbers of quarks [31, 32]	7
3.1	BEPC operating parameters after its first upgrade ([37], [38]).	18
5.1	The background estimates for $\psi(2S) \rightarrow \Omega^-\bar{\Omega}^+, \Omega^- \rightarrow \Lambda K^-, \bar{\Omega}^+ \rightarrow$ $\bar{\Lambda}K^+$ [83]	62
5.2	Systematic uncertainties (%) in the branching fraction ([82], [83])	77

Chapter 1

INTRODUCTION

High energy physics [1, 2] deals with theoretical as well as experimental techniques for studying fundamental particles and their interactions. Theoretical approach includes mainly the mathematical framework of quantum field theories ([3], [4], [5], [6], [7], [8], [9], [10]). On the experimental side, to probe the fundamental issues of the universe, the accelerator and detector technology is playing an extremely important role ([11], [12], [13], [14], [15]).

In high energy physics laboratories, complexity of fundamental physics is investigated, by running either fixed target ([16], [17], [18]) or collider experiments in desired energy range ([11], [12], [13], [14], [15]). In these experiments, available energy of the system is used to examine fundamental particles (quarks and leptons) and their properties. Quarks have never been observed directly by the detectors [19, 20]. Instead, their signatures are left in the form of their bound states called hadrons: baryons and mesons [21, 22]. Hadrons are both stable or unstable. The unstable ones decay into

stable products that are observed directly by the detectors. Direct observations of stable particles by the detectors, after necessary processing, are used to reconstruct physics of their primary hadronic sources ([23], [24], [25]). Physical aspects of partons: quarks, antiquarks and gluons, are approximated, through characteristic study of hadrons.

Among quark categories, Charm quark is of great importance. It is the first heavy quark. Its properties can play a prototype role for other two heavy quarks: bottom and top. At Charm Factories (such as SLAC, CLEO and BES), properties of Charm quark and its antiquark are investigated through study of their bound states: the charmonia [26]. $\psi(2S)$ is one of these states whose decay dynamics is investigated to determine physical quantities such as probability of Ω^- production in $\psi(2S)$ decays. We have studied $\psi(2S) \rightarrow \Omega^- \bar{\Omega}^+$ decay process, using 14×10^6 $\psi(2S)$ decays recorded by BESII detector at Beijing Electron Positron Collider (BEPC) storage ring [27]. Analysis has been performed using dominant decay modes of Ω^- and $\bar{\Omega}^+$ i.e., $\Omega^- \rightarrow \Lambda K^-$ and $\bar{\Omega}^+ \rightarrow \bar{\Lambda} K^+$. Using a new analysis approach of selecting events with one missing charge track also, first evidence of $\psi(2S) \rightarrow \Omega^- \bar{\Omega}^+$ is reported, with Ω^- and $\bar{\Omega}^+$ having statistical significance levels of 5.3σ and 4.6σ , respectively. A branching fraction of this decay process is determined to be $(3.21 \pm 1.25 \pm 0.97) \times 10^{-5}$. The errors are statistical and systematic, respectively. Analysis details of this study are provided in chapter 5. Before that, first of all, in chapter 2, we go through main concepts of particle physics, especially meson and baryon multiplets, within the quark model. The BESII experimental setup used for recording 14 million $\psi(2S)$ data is

described in third chapter. In fourth chapter we make a brief literature survey of electron positron annihilations with special reference to formation of charmonium states and their decays. In this chapter, important decay aspects of Ω^- and $\bar{\Omega}^+$ are also discussed. In last chapter we discuss the analysis approach, physics results and draw conclusions in a future perspective.

Chapter 2

PARTICLES AND THEIR INTERACTIONS

Standard Model of Particle Physics, provides the best approach for understanding of important physical aspects of fundamental particles and laws governing their interactions [28, 29]. A brief of preliminary concepts, is given in the following sections.

2.1 Fundamental Particles

Basic constituents of matter comprise of twelve fundamental fermions (spin-1/2 particles); six quarks and six leptons. Quark flavors are: up (u), down (d), strange (s), charm (c), bottom (b) and top (t) whereas leptons include: electron (e^-), electron-neutrino (ν_e), muon (μ^-), muon-neutrino (ν_μ), tau (τ^-) and tau-neutrino (ν_τ). Corresponding to these fundamental particles, there are six antiquarks: anti-up (\bar{u}), anti-down (\bar{d}), anti-strange (\bar{s}), anti-charm (\bar{c}), anti-bottom (\bar{b}) and anti-top (\bar{t}), and six

antileptons: anti-electron or positron (e^+), anti-electron neutrino or positron-neutrino ($\bar{\nu}_e$), anti-muon (μ^+), anti-muon neutrino ($\bar{\nu}_\mu$), anti-tau (τ^+) and anti-tau neutrino ($\bar{\nu}_\tau$). In each such pair, particle and antiparticle have equal masses but equal and opposite quantum numbers like; electric charge(Q), lepton number(L), baryon number(B), etc.

Electrically charged leptons and antileptons experience electromagnetic as well as weak force whereas neutral ones experience only weak interaction. Each candidate of lepton family is assigned a lepton quantum number according to its generation; electron lepton number of 1 ($L_e = 1$) for e^- and ν_e , muon lepton number of 1 ($L_\mu = 1$) for μ^- and ν_μ and tau lepton number of 1 ($L_\tau = 1$) for τ^- and ν_τ . Corresponding to each lepton generation, an antilepton generation is assigned a lepton quantum number of -1. In this way, there are three separate conservation rules regarding; 'electron lepton number', 'muon lepton number' and 'tau lepton number', found satisfied one by one in all electroweak processes, provided the corresponding neutrinos are massless [30, 31]. Additive quantum numbers along with mass estimates for known lepton generations are given in Table 2.1.

Each quark flavor, in addition to the electric and weak charges, is assigned a color charge, which accounts for strong interaction among the quarks. By convention, quarks are assigned positive parity whereas antiquarks negative. In addition, quarks have a baryon quantum number 1/3 and anti-quarks -1/3. Main additive quantum numbers of quark flavors along with their constituent quark masses, are listed in Table 2.2. These quantum numbers are related to charge Q of any quark flavor through

Table 2.1: Additive quantum numbers of leptons [30, 32]

	Q	L_e	L_μ	L_τ	Mass (MeV/ c^2)
e^-	-1	+1	0	0	= 0.511
ν_e	0	+1	0	0	≤ 0.01
μ^-	-1	0	+1	0	= 105.66
ν_μ	0	0	+1	0	≤ 0.16
τ^-	-1	0	0	+1	= 1777
ν_τ	0	0	0	+1	≤ 18

generalized Gell-Mann-Nishijima formula:

$$Q = I_z + \frac{B + S + C + Bt + T}{2},$$

where I_z , B , C , Bt and T denote the quantum numbers: z-component of isospin, Baryoness, Charmness, Bottomness, and Topness respectively. Conventionally, their signs are taken as those of their electric charge Q [31].

2.2 Fundamental Interactions

Fundamental particles can interact through Strong, Weak, Electromagnetic and Gravitational forces. Two of these forces; Electromagnetic and Weak, unified into ElectroWeak force are studied in the framework provided by ElectroWeak theory [29] (also known as the minimal Standard Model). The strong force is investigated in a

Table 2.2: Additive quantum numbers of quarks [31, 32]

	d	u	s	c	b	t
Electric Charge (Q)	$-\frac{1}{3}$	$+\frac{2}{3}$	$-\frac{1}{3}$	$+\frac{2}{3}$	$-\frac{1}{3}$	$+\frac{2}{3}$
Isospin (I)	$\frac{1}{2}$	$\frac{1}{2}$	0	0	0	0
Isospin z-component (I_z)	$-\frac{1}{2}$	$+\frac{1}{2}$	0	0	0	0
Strangeness (S)	0	0	-1	0	0	0
Charmness (C)	0	0	0	+1	0	0
Bottomness (Bt)	0	0	0	0	-1	0
Topness (T)	0	0	0	0	0	+1
Constituent Quark Mass (GeV/c^2)	$\simeq 0.31$	$\simeq 0.31$	$\simeq 0.50$	$\simeq 1.6$	$\simeq 4.6$	$\simeq 180$

theory called Quantum Chromodynamics (QCD) [29]. The extended Standard Model includes ElectroWeak theory and Quantum Chromodynamics. The gravitational force is not a part of the Standard Model. The forces are mediated through exchange of intermediate particles of integer spin, called gauge bosons. Electromagnetic force is mediated through photon (γ). All the extra-nuclear physics such as; binding of electrons with the nuclei and the intermolecular interactions in liquids and solids, are due to electromagnetic force. Weak force is mediated through W^\pm and Z^0 . Its typical example is slow nuclear β -decay process in which a radioactive nucleus emits an electron and its antineutrino. Strong force is mediated through gluons. Mediating gluons themselves have color charge and consequently interact strongly. The strong force is responsible for keeping quarks and antiquarks bound inside hadrons [29]. The Gravitational interaction is assumed to mediate through exchange of spin 2 gauge bosons called gravitons. All the particles with non zero mass experience this force. At quantum level, the strength of gravitational force is negligibly smaller as compared to the strengths of other three forces. A rough comparison among the strengths of these forces, for two protons just in contact, is as follows [32]:

$$\begin{array}{cccc}
 \textit{Strong} & \textit{Electromagnetic} & \textit{Weak} & \textit{Gravity} \\
 a & a \times 10^{-2} & a \times 10^{-7} & a \times 10^{-39}
 \end{array} ,$$

where a is the strength of strong force between the two protons. The comparison indicates that the strong force is the prominent one. The hadrons formed under the action of this force are categorized according to their quantum numbers.

As $\psi(2S) \rightarrow \Omega^- \bar{\Omega}^+$ involves mesons as well as baryons, it is important to know their nature and properties amongst the known hadron families. For this purpose, in the

following two sections, we will explain the way hadrons are classified based upon their properties acquired from constituent quarks and/or antiquarks.

2.3 Mesons

In quark model, bound state of a quark and an antiquark; $q\bar{q}'$, is called meson, where q and \bar{q}' may be of same or different flavors. As quarks have baryon number $1/3$ and antiquarks $-1/3$, mesons have baryon number zero. Total angular momentum J (in this case spin) of a meson arises from its orbital angular momentum and spin angular momentum of quark antiquark pair: $J = L + S$. Spin angular momentum quantum number j satisfies the inequality $|l-s| \leq j \leq |l+s|$, where l is orbital angular momentum quantum number and s is spin quantum number. As quark and antiquark may be aligned or anti-aligned, s has two values: 0 and 1. Parity and C-parity or charge conjugation of a meson are evaluated using the relations: $P = (-1)^{l+1}$ and $C = (-1)^{l+s}$. When isospin I of meson is also considered, relation for C-parity is generalized to G-parity: $G = (-1)^{I+l+s}$. Ground state mesons with $l = 0$ and $s = 0$, are called *pseudoscalar* mesons and their parity and C-parity are found to be -1 and $+1$, respectively, giving $j^{PC} = 0^{-+}$. For $l = 0$ and $s = 1$, set of states is called *vector* mesons for which $j^{PC} = 1^{-}$. For excited state mesons with $n \geq 2$, where n is principal quantum number and $l = 0, 1, 2, \dots, n-1$, j^{PC} values are obtained in the same way. Mesons with same j^{PC} values are placed in same group called meson *multiplet*. In this way, for three quark flavors: up, down and strange, for each of the ground and excited states, there exists a *nonet* of mesons. The ground state mesons

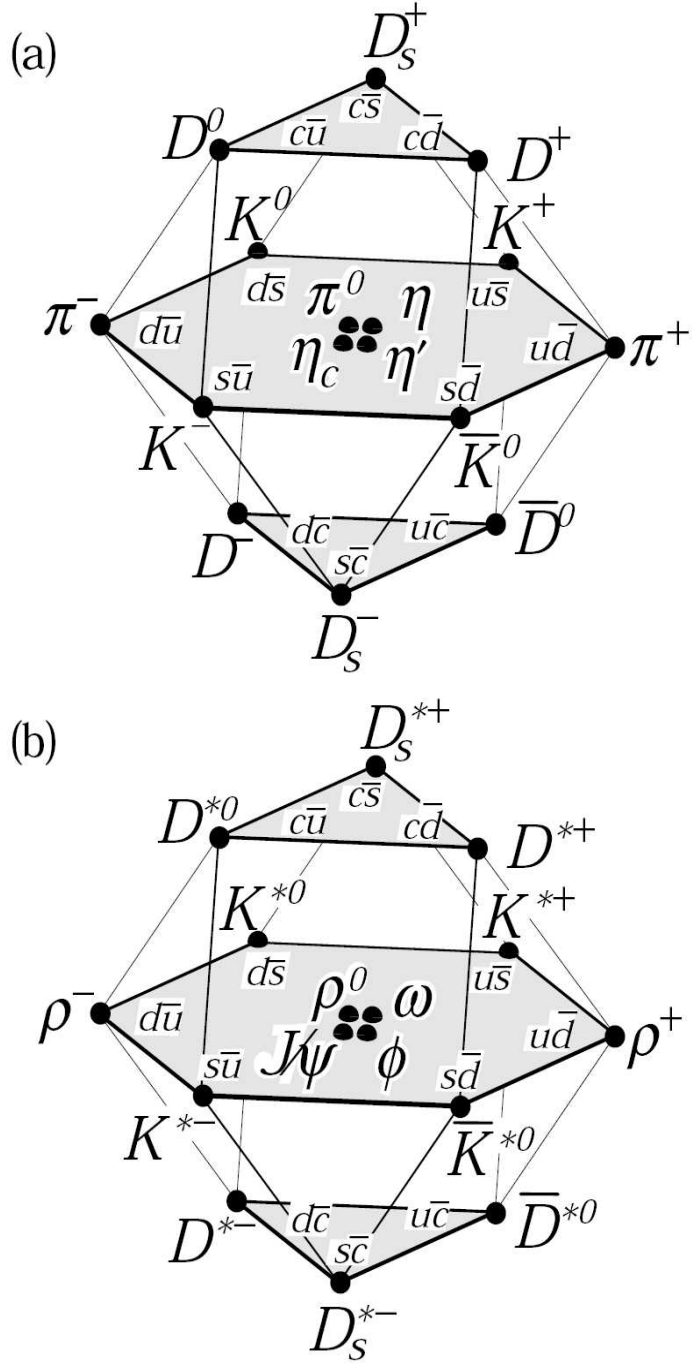


Figure 2.1: SU(4) meson multiplets made of up, down, strange and charm quark flavors. (a) SU(4) 16-plet for pseudoscalar mesons and (b) SU(4) 16-plet for vector mesons. The nonets of pseudoscalar and vector light mesons make the central planes. These planes also contain $c\bar{c}$ states [31].

with $l = 0$ and $s = 0$, have three possibilities of strangeness: 0, +1 and -1. For isospin, there are three possible values: 0, +1 and 1/2. With zero strangeness, there will be five $q\bar{q}'$ combinations including: $u\bar{u}$, $d\bar{d}$, $u\bar{d}$, $d\bar{u}$ and $s\bar{s}$. They are subgrouped using their isospin values i.e. 0 or +1. For isospin +1, there is a triplet of states: π^0 ($I_z = 0$), π^- ($I_z = -1$) and π^+ ($I_z = +1$). For isospin zero, there exist two isospin singlet states called eta (η) and eta-prime (η') which are mixture of $u\bar{u}$, $d\bar{d}$ and $s\bar{s}$ combinations. With strangeness +1 and isospin +1/2, there is a doublet of states: K^+ ($I_z = +1/2$) and K^0 ($I_z = -1/2$). There is another doublet, for which isospin is +1/2 and strangeness is -1: K^- ($I_z = -1/2$) and \bar{K}^0 ($I_z = +1/2$). In this way, a *nonet* of the pseudoscalar mesons is obtained [33]. For vector mesons; $l = 0$, $s = 1$ thus $j = 1$, in one-to-one correspondence with the pseudoscalar mesons, there exists a *nonet* [33].

When charm quark is included by extending SU(3) to SU(4), due to its much larger mass, SU(4) is badly broken. By plotting third component of isospin, hypercharge and charmness of sixteen mesons in SU(4) classification, the weight diagrams for ground state pseudoscalar mesons with $j^{PC} = 0^{-+}$ and ground state vector mesons with $j^{PC} = 1^{-}$, are as shown in Fig. 2.1 [31]. These diagrams contain 16-plets of pseudoscalar scalar mesons and vector mesons. SU(3) nonets of ground state pseudoscalar and vector mesons are found lying in central planes of the weight diagrams. Final state pseudoscalar mesons of our decay channel; π^+ , π^- , K^+ and K^- are in the central plane of Fig. 2.1 (a).

We can also see that among the vector mesons, there is also a charmonium ($c\bar{c}$) state

called J/ψ or $\psi(1S)$ with mass of 3.097 GeV. It was discovered simultaneously at BNL [34] and SLAC [35], in 1974. After ten days, another resonance: $\psi(2S)$ (first excited state of J/ψ) with a mass of 3.686 GeV, was also discovered at SLAC.

2.4 Baryons

Bound state of three quarks is called baryon. As quarks are fermions, baryons themselves also acquire fermionic nature. Total angular momentum of a baryon called its spin (J), comes from its orbital angular momentum (L) and total spin of its constituent quarks (S). Possible values for orbital angular quantum number l are 0, 1, 2, and so on. For $l = 0$, total spin angular momentum quantum number for a baryon, is either $1/2$ (two quarks aligned and one anti-aligned) or $3/2$ (all three quarks aligned). With three quark flavors; up, down and strange, an octet and a decuplet of baryons is obtained, for spin $1/2$ and $3/2$, respectively. The octet is sub-grouped depending upon isospin and strangeness of baryons. For zero strangeness and isospin $1/2$, there are four quark configurations i.e., uuu , ddd , uud and udd . Two of them; uuu and ddd , are forbidden by Pauli's exclusion principle. Thus only two states; proton (uud) and neutron (udd), are possible. With strangeness -1 and isospin 1, there are three allowed states; Σ^- (dds), Σ^0 (uds) and Σ^+ (uus). With zero isospin and one strange quark, the hadron formed is Λ^0 (uds) baryon. Remaining baryonic states: Ξ^- (dss) and Ξ^0 (uss), have strangeness -2 and isospin $1/2$. In this way, an octet of ground state baryons with $J^P = \frac{1}{2}^+$ is obtained (+ indicating space symmetry of baryon wave function) [33].

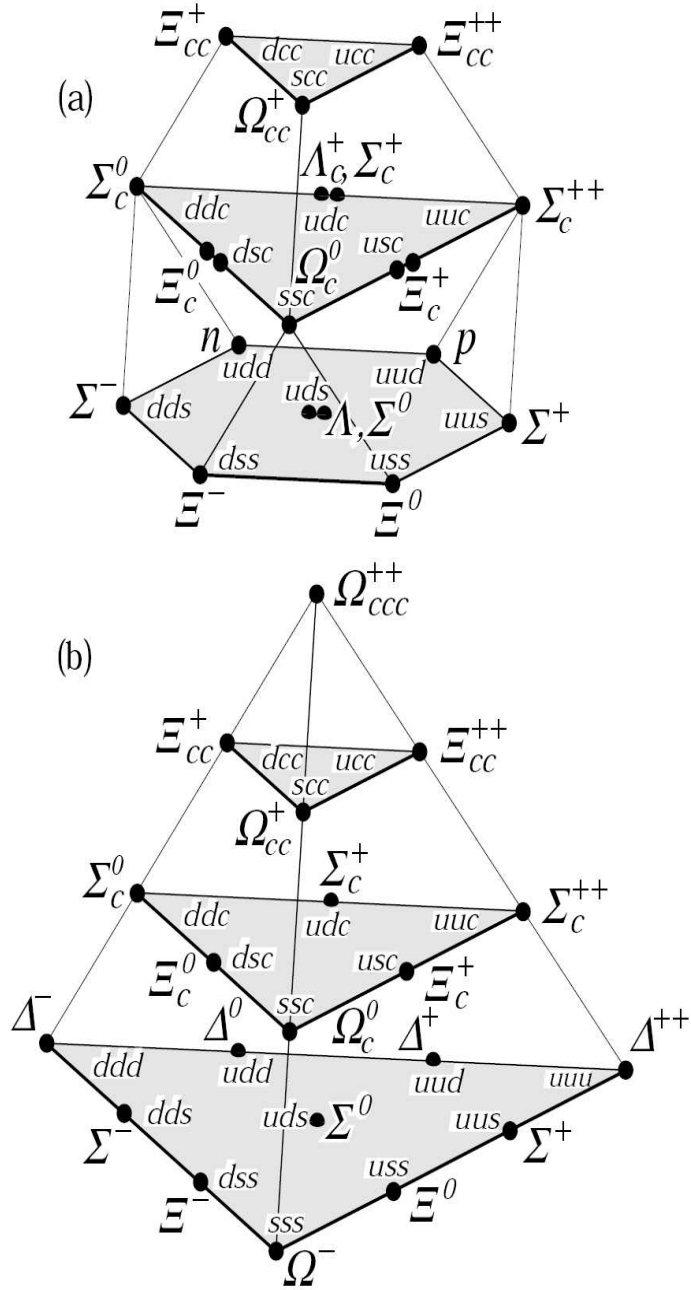


Figure 2.2: SU(4) baryon multiplets made of up, down, strange and charm quarks. (a) The 20-plet with an SU(3) baryon octet. (b) The 20-plet with an SU(3) baryon decuplet [31].

For baryons with spin $3/2$, there is a decuplet or decimet. With zero strangeness and isospin $3/2$, a quartet of baryons; Δ^- (ddd), Δ^0 (udd), Δ^+ (uud) and Δ^{++} (uuu) is formed. With strangeness -1 and isospin 1 , the baryons are Σ^{*-} (dss), Σ^{*0} (uds) and Σ^{*+} (uus). With strangeness -2 and isospin $1/2$, the baryons found, are Ξ^{*-} (dss) and Ξ^{*0} (uss). Very unique and isospin singlet state with strangeness -3 , is the Ω^- baryon [33].

When c quark is also considered, due to its larger mass as compared to light quarks, flavor symmetry $SU(4)$ is badly broken. $SU(4)$ multiplets, containing octet and decuplet of $SU(3)$, are shown in Fig. 2.2. $SU(3)$ octet and decuplet of baryons form the lowest planes of $SU(4)$ multiplets [31]. Ω^- baryon is found at corner of the lowest plane in Fig. 2.2 (b). Antibaryons; antilambda ($\bar{\Lambda}$), antiproton (\bar{p}) and antiomega ($\bar{\Omega}^+$), can be found in octet and decuplet obtained from three antiquark flavors; anti-up (\bar{u}), anti-down (\bar{d}) and anti-strange (\bar{s}).

In following subsection, we highlight significance of Ω^- baryon, with special reference to credibility of quark model and color charge.

2.4.1 Discovery of Ω^- and its Physical Significance

According to quark model scheme, there are quark configurations; uuu and sss , that match the properties of baryons: Δ^{++} (observed in 1951 by Fermi and collaborators) and Ω^- respectively. Δ^{++} baryon with spin $+3/2$ was assumed forbidden by Fermi-Dirac statistics as it is only possible if three up quarks (spin $1/2$) are aligned in their ground state ($l = 0$). In addition to other problems faced by the quark model, this

fiasco was resolved by introducing 'color' quantum number for quarks, making three up quarks distinguishable from each other such as $u_R u_G u_B$. After mass and decay modes of Ω^- were predicted by quark model, it was searched for and thus discovered in 1964 at Brookhaven National Laboratory (BNL) in a strong reaction: $K^- + p \rightarrow \Omega^- + K^+ + K^0$, ten years before discovery of first charmonium state. Therefore, first predicting properties of Ω^- and then observing it accordingly was no less than a crowning achievement of quark model. As properties of Ω^- baryon match those of sss quark configuration, its discovery further strengthened the belief in color charge and thus in QCD. Searching for and thus observing Ω^- in $\psi(2S)$ decays will further enhance the credibility of quark model as well as QCD [33, 36]. In our work, we report a first evidence of Ω^- and $\bar{\Omega}^+$ through analysis of $\psi(2S) \rightarrow \Omega^- \bar{\Omega}^+$ using 14 million $\psi(2S)$ decay events recorded by BESII experiment. Functional parts of this experiment are described in the next chapter.

Chapter 3

EXPERIMENTAL SETUP

In this chapter, we will begin with a brief overview of BEPC. We then move on to highlight functional parts of BESII detector. At the end, a brief of; luminosity measurements, detector background and detector performance has been included. Detailed description has been avoided which is available in scholarly work such as [37], [38] and [39].

3.1 Beijing Electron Positron Collider

Beijing Electron Positron Collider is situated on grounds of Institute of High Energy Physics (IHEP) located on western outskirts of Beijing [27]. It was originally constructed between 1984 and 1988. Its first upgrading was carried out from 1993 to 1997, involving; reduction in horizontal beta function (β_x^*), replacement of Aluminum beam pipe with Beryllium beam pipe in interaction region of BES detector, introduction of a separator at second interaction point (IP) etc [37]. Operating parameters

of BEPC, after first upgrading, are shown in Table 3.1 [37], [38], [39], [40], [41], [42]. Its schematic layout is shown in Fig. 3.1. Mr. Derrick Kong, in his Ph.D thesis [37] nicely described a detailed working of BEPC and BESII detector. A brief description of the same is given below:

A 30 MeV Pre-injector ejects pulses of electrons to 120 MeV linear accelerator. These pulses are injected into main linac or fired on a fixed target to produce positrons. Main linac further accelerates the pulses to desired energy before sending them into storage ring. Positrons are also accelerated in the same way before they are sent into storage ring. Inside storage ring, beams of electrons and positrons rotate opposite to each other. Once a particular luminosity level is reached, they are collided at center of BESII detector, called Interaction Point (IP).

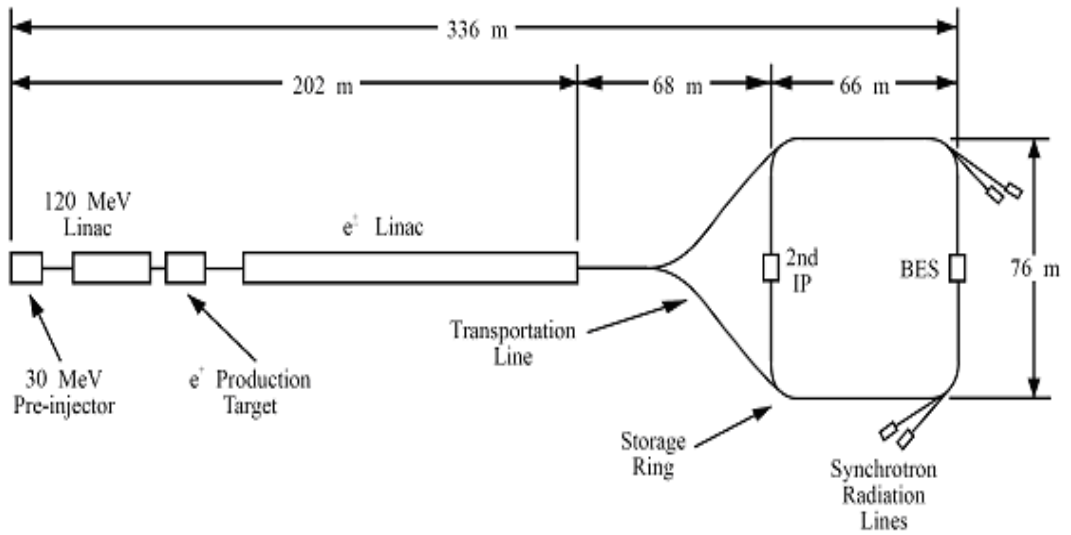


Figure 3.1: Schematic diagram of Beijing Electron Positron Collider [37]

Table 3.1: BEPC operating parameters after its first upgrade ([37], [38]).

Beam life time	T	(6 – 8) h
Beam momentum	$p_{e\pm}$	(1.0 – 2.5) GeV/c
Center of mass energy	E	(2 – 5) GeV
Energy spread	$\Delta E/E$	2.64×10^{-4}
Circumference of storage ring	C	240.4 m
Bunch spacing	t_b	801.888 ns
Natural length of a bunch	σ_l	5.2 cm
Frequency of revolution	f_0	1247.057 KHz
Horizontal Beta function at interaction point	β_x	103.0 cm
Vertical Beta function	β_y	5.5 cm
Size of horizontal spot at point of interaction	σ_y	38.7 μm
Number of particles in one bunch at injection point	N_b	6.8×10^{10}
Beam-Beam inner radius at interaction point	r	7.5 cm

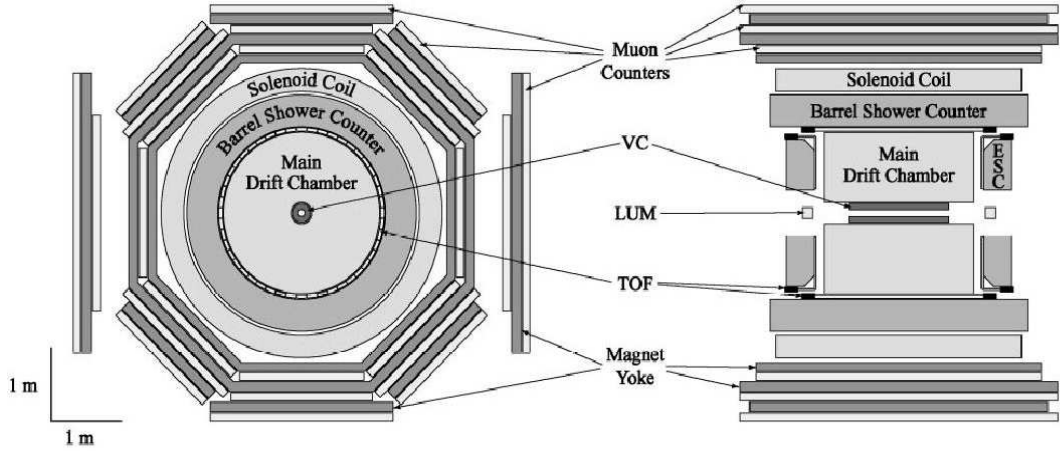


Figure 3.2: Side and end views of BESII detector ([38], [39]).

3.2 BESII Detector

BESII detector, was operated from 1997 to 2002. It is classified as a conventional solenoidal detector [41]. Its side and end views are shown in Fig.3.2 ([38], [39]). During its operation, energies of electron and positron beams were adjusted such that center of mass system and laboratory system coincided with each other. Center of mass energy of colliding beams; $(2 - 5)$ GeV was ranged over charmonium states: $J/\psi(1S)$, $\psi(2S)$ and $\psi(3S)$. Decay events of these vector charmonia have been measured by BES I as well as BESII detectors. Charmonium data thus obtained has been analyzed for study of: hadron production, open charm ($D\bar{D}$) production and $\tau^+\tau^-$ production [38]. Analysis results reported in this thesis were determined using about 14 million $\psi(2S)$ events recorded by BESII detector from 2001 to 2002 ([38], [43]), with an integrated luminosity of $(19.72 \pm 0.86) pb^{-1}$ ([38], [44]).

3.2.1 Beam Pipe

As described by Mr. Derrick Kong [37], beam pipe lies at core of BES detector. Electrons and positrons move in an evacuated path provided by it. Ideally its thickness should be as small as possible and material properties should be in favor of low particle scattering as well as reduced photon pair conversion. In the upgrade process, a beryllium pipe having 9.8 cm diameter and 1.2 mm thickness was introduced in place of original aluminum pipe.

3.2.2 Vertex Chamber

In BESII detector, outside the beam pipe, was vertex chamber (VC) [37]. Its main purpose was to provide information about event vertices. Its operation in conjunction with main drift chamber (MDC), was used to improve tracking acceptance and momentum resolution. It was introduced after refurbishment of original vertex chamber used in MARK III detector [45]. There were 12 layers containing 640 straws within inner and outer diameters of 10.8 cm and 26 cm respectively. These layers were divided into three sections; from 1 to 4 and 9 to 12 were axial layers whereas from 5 to 8 were stereo type layers at an angle of about 3 degrees with the beam axis. Vertex chamber was designed to operate up to 5 atmospheric pressure in Ar/C₂H₆ (50%/50%) working gas, but it worked at 3 atmospheric pressure and with a voltage from 3.7 to 3.9 kV. Its average single hit resolutions for cosmic rays and colliding beam data, are $(73.4 \pm 8.4) \mu m$ and $90 \mu m$, respectively.

3.2.3 Main Drift Chamber

Just outside the vertex chamber of BESII detector was main drift chamber (MDC) [37]. This is main tracking part of detector that provides information about gas ionization effects of charged particles, to reconstruct particle tracks with great precision. Along with reconstruction of tracks, their bending inside the uniform magnetic field is used to measure momentum values.

Like VC, it also has concentric cylindrical structure. Inner and outer radii of MDC are 31 cm and 230 cm, respectively. Effective length of MDC is 212 cm, inside tensioned endplates of 4 cm thickness. BESII MDC had ten tracking layers provided with 22,936 axial and stereo wires. These wires were arranged in 804 cells; ranging in number from 48 to 128 in innermost layer to outermost layer. Even layers were used to hold axial wires whereas odd layers were equipped with stereo wires; making small angle with cylindrical axis. Wires were used for four tasks; 3,216 sense wires for reading out signals, 11,468 field wires for providing constant electric field, 5,308 potential wires for maintaining separation between sense wires, reducing cross-talk and enhancing stability and 2,944 guard wires to reduce field distortions at edges of layers. Each layer had some level of symmetry; first four layers had eight-fold symmetry whereas remaining six layers had four-fold symmetry. Working gases inside MDC were Ar/CO₂/CH₄ (89%/10%/1%). Solid angle coverage range was from 95% of 4π for second layer to 70% of 4π , for tenth layer. Single wire efficiency was in range of 85% – 95% with resolution of 198 – 224 μ m in $r - \phi$ plane. Momentum values measured for charge tracks had a resolution: $\Delta p/p = 1.78\% \sqrt{1 + p^2}$, where

p is momentum in GeV/c . Very important characteristic of MDC is resolution of measured values of energy loss of charged particles moving through it, as a function of particle momentum. Energy loss information as a function of distance traveled (dE/dx) can be used to identify particles, because it depends upon mass of charged particle. Performance of MDC of BESII detector, in particle identification through dE/dx information is shown in Fig. 3.3.

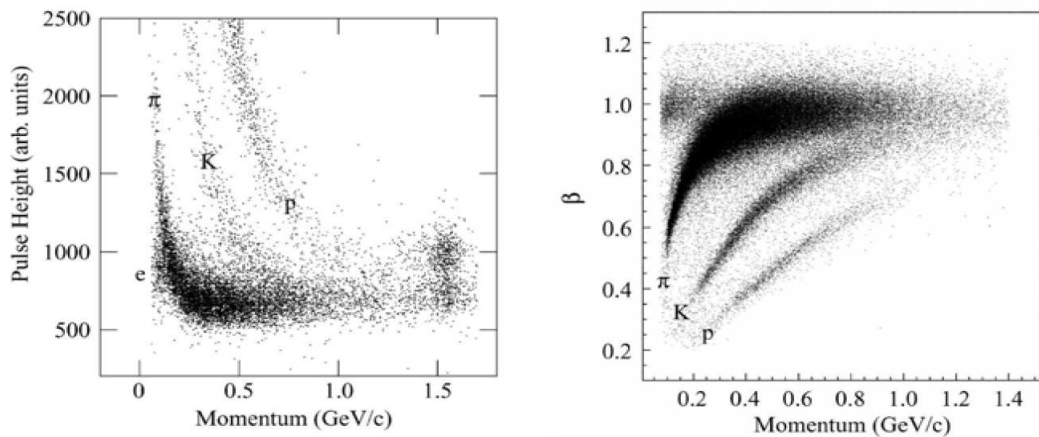


Figure 3.3: dE/dx (left) and TOF (right) resolutions at BESII [38], [39]

dE/dx resolution as measured via Bhabha events is 8.0%. From Fig. 3.3, it is clear that K/π and p/K separation through dE/dx information is inefficient for momentum values greater than 600 MeV/c and 900 MeV/c , respectively.

3.2.4 Time-of-Flight (TOF) System

Particle identification can be performed by using ionization energy loss (dE/dx) as well as time of flight information of charged particles passing through MDC and then hitting detector part responsible for measuring time of flight of particles. In

order to measure time of flight, BESII Time-of-Flight (TOF) system (just outside MDC) was divided into two categories; Barrel TOF and End-Cap TOF [37]. Basic response elements in TOF were plastic scintillation counters whose output light is passed on to a photomultiplier tube (PMT) via a clear Lucite light pipe. Barrel TOF system was provided with 48 BC408 scintillation counters, arranged in cylindrical shape, having length, width and thickness of 284 cm, 15.6 cm and 5 cm, respectively. End-cap TOF system had two plates, each with 24 NE110 scintillation counters of trapezoidal shape, with a height of 70 cm and width in range of 9 – 27.45 cm. End-cap TOF system specifications were same as that of BESII end-cap TOF system. As photomultiplier tubes were in magnetic field of solenoid, they were designed in such a way so as to resist magnetic field effects. Time of flight resolutions for Bhabha events ($e^+e^- \rightarrow e^+e^-$) and hadronic events, were 180 ps [46] and 200 ps, respectively, good enough for separation among proton p , kaon K and pion π , for momenta less than 1 GeV/c. TOF resolution at BESII is shown in Fig. 3.3.

3.2.5 Electromagnetic Shower Counter

An electromagnetic shower counter system just outside the TOF system of BESII detector, was used to measure energies of photons and electrons passing through it. This detector part was divided into two sections; barrel shower counter (BSC) and end-cap shower counter (ESC). The BSC had twenty four layers made of self quenching streamer (SQS) mode tubes, covering 80% of the solid angle. The BSC layers were interleaved with 24 layers of lead absorber, each of 0.5 radiation length.

Thus whole BSC was capable of providing 12 radiation lengths. The BSC made energy and spatial measurements with resolutions: $\sigma_E/E = 0.22/\sqrt{E}$ (E in GeV) and $\sigma_\phi = 4.5$ mrad, $\sigma_\theta = 12$ mrad, respectively ([37], [38]).

3.2.6 Muon Counter

This is the outermost BESII sub-detector, adjacent to solenoidal magnetic coil. It had three layers interleaved with iron flux return. Its function was to register signals of muons having momentum greater than 0.5 GeV/c. Axial proportional tubes were employed for measuring muon track position in ϕ and charge division was used to determine z-coordinate of muon tracks ([37], [38]).

3.3 Luminosity Measurements

Perturbative Quantum Electrodynamics (PQED) can be used to calculate small angle scattering of electrons and positrons. Comparison between such theoretical calculation and BESII measurement was used to determine luminosity with an uncertainty of 3%. However, the number of $\psi(2S)$ events was determined in a different way: first finding number of data events of $\psi(2S) \rightarrow J/\psi\pi^+\pi^-$ and then dividing the result by known branching fraction of this channel [38].

3.4 Detector Background

Detector background arises mainly from two sources: noisy electronics channels and signal distortion due to unwanted interactions of decay particles with the detector. Such background varies from experiment to experiment. In BESII, the signal distortion due to unwanted small angle scattering, energy losses, bremsstrahlung, pair production and electronics deficiencies, is taken into account in Monte Carlo simulation [38].

3.5 Detector Performance

BESII detector performance has been checked through its Monte Carlo simulations based upon SIMBES (a GEANT3 based program). In these simulations, detector geometry and its response has been considered in detail. A reasonable consistency has been found between data and Monte Carlo for many J/ψ and $\psi(2S)$ decays. Details can be found in Ref. [47].

To review charmonium production (especially $\psi(2S)$), with special reference to electron positron annihilations, followed by hadron production, such as $\Omega^-\bar{\Omega}^+$, we move to the next chapter.

Chapter 4

LITERATURE REVIEW

4.1 Electron Positron Collisions

¹In electron positron collisions, lepton antilepton or quark antiquark pairs are produced in a clean environment. Having enough energy, these pairs make electroweak or strong radiation. Consequent production of particles leads to 'final state particles'. The final state information registered by a detector is used to reconstruct physics of 'parent particles'. The information thus obtained help in understanding the nature of electroweak or strong interactions [36]. Information about the primary resonance is therefore reconstructed by mapping the entire decay process. For conclusive physics results, we need to analyze a large sample of decay events of that resonance. The sample is normally obtained through interaction of colliding beams at a particular center

¹The material in this chapter is not original and has primarily been taken from the scholarly work cited in references. In view of the large amount of resource available in literature, many details have not been included which are available on hep archives. Author apologizes to all whose scholarly work could not be included or get the due share.

of mass energy. Electron positron collider experiments at CLEO-c [48] and BESII [47] have reported several interesting results about hadron spectroscopy. An upgrade at BEPC of electron positron collision experiment, BESIII (<http://bes3.ihep.ac.cn/>), has started providing samples of charmonium states: J/ψ and $\psi(2S)$. This experiment will provide huge samples of charmonium states for exploring new physics including precise measurements of interesting hadronic properties. During the past three decade, a lot of work has been reported on experimental and theoretical side. In this chapter we will give a brief sketch of the progress made so far. In doing so, we primarily rely on the scholarly work detailed in references ([36], [47], [48] – [81]) without undermining the contribution of all others whose work is not cited directly due to paucity of space.

4.1.1 Hadron Production

In electron positron collisions, the main process in hadron production is the leading order process; $e^+e^- \rightarrow q\bar{q}$. Other higher order processes like; $e^+e^- \rightarrow q\bar{q}g$, $e^+e^- \rightarrow q\bar{q}gg$, $e^+e^- \rightarrow q\bar{q}ggg$, etc have very low contribution to the hadron production at low energies. Therefore, the leading order process is of special interest. The total cross section for the hadron production from quark antiquark pair produced can be readily obtained in analogy with the leading order QED process; $e^+e^- \rightarrow \mu^+\mu^-$ whose cross section is given as [36]:

$$\sigma(e^+e^- \rightarrow \mu^+\mu^-) = \frac{4\pi\alpha^2}{3s}, \quad (4.1)$$

where s and α are the squared center of mass energy of colliding electron and positron and electromagnetic coupling constant, respectively. Taking into account the fractional charges of quarks & antiquarks and their color charge, the cross section for hadron production from a quark flavor is given as:

$$\sigma(e^+e^- \rightarrow q\bar{q}) = 3e_q^2 \frac{4\pi\alpha^2}{3s},$$

where e_q represents the charge of a quark flavor. When all the quark flavors are considered for hadron production, the total cross section becomes:

$$\sigma(e^+e^- \rightarrow q\bar{q}) = 3 \sum_q e_q^2 \frac{4\pi\alpha^2}{3s}$$

The above cross section can be written as:

$$\sigma(e^+e^- \rightarrow \text{hadrons}) = 3 \sum_q e_q^2 \times \sigma(e^+e^- \rightarrow \mu^+\mu^-),$$

leading to an important ratio:

$$R = \frac{\sigma_{e^+e^- \rightarrow \text{hadrons}}}{\sigma_{e^+e^- \rightarrow \mu^+\mu^-}} = 3 \sum_q e_q^2$$

This result helps in obtaining information about the number of quarks, their flavors and (three) colors [36]. It has been verified by comparing the predicted values of R with the experimental data. In charmonium mass region, the ratio R versus \sqrt{s} ([38], [49]) is shown in Fig. 4.1.

Having studied hadron production briefly, we now take up charmonium states and their related physics.

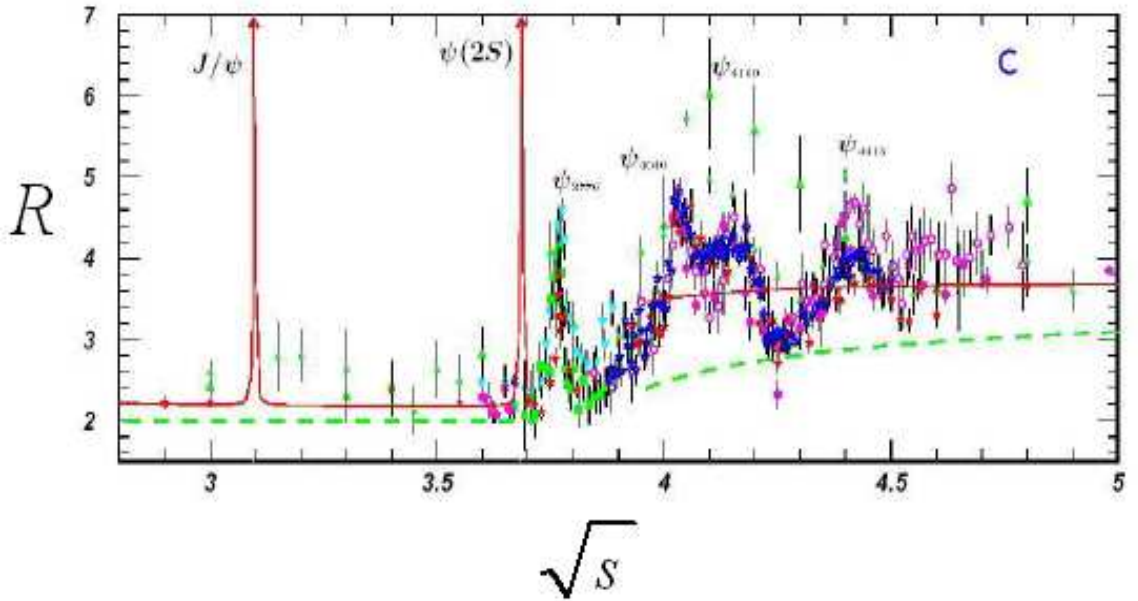


Figure 4.1: Ratio R as a function of center of mass energy \sqrt{s} , in the charmonium mass region ([38], [49]).

4.2 Charmonium States

A Charmonium is a meson containing a charm quark anti-quark pair ($c\bar{c}$). Charm flavor of quarks was confirmed after a charmonium candidate, with central mass value $\approx 3.097 \text{ GeV}/c^2$, was discovered simultaneously at BNL [34] and SLAC [35] in November, 1974 (known as 'November Revolution' in history of particle physics). The SLAC and BNL groups named this particle, ψ and J , respectively. Therefore, in literature, this resonance is known by the combined name, J/ψ . At SLAC, this resonance was discovered in the following process:

$$e^+ + e^- \rightarrow \psi \rightarrow \text{hadrons} [33],$$

where as BNL group observed this resonance in the following process:

$$p + Be \rightarrow J + X, \quad J \rightarrow e^+ + e^- [33].$$

In both observations, the central mass value and upper limit on the decay width were determined, providing a convincing evidence of the resonance being studied [33]. Natural width of this particle was measured to be about 63 KeV, indicating long lifetime of this resonance. J/ψ is the lowest energy charmonium state with principal quantum number $n = 1$, orbital angular momentum quantum number $l = 0$, intrinsic angular momentum quantum number $s = 1$ and total angular momentum quantum number $j = 1$. Parity and C-parity of this state were determined as $j^{PC} = 1^{--}$.

A charmonium state is a simplest bound state in QCD. In analogy with positronium or a Hydrogen atom, there exists a series of charmonium resonances for allowed excited states of $c\bar{c}$ pair, characterized by the quantum numbers n, l, s, j, P and C . Such states: $\psi(3097), \psi(3686), \psi(3770), \psi(4040), \psi(4170)$ (radial excitations with different principal quantum number but with same $l = 0$ and $j = 1$) and so on. These states can be produced in electron positron annihilation because their j^{PC} is conserved. According to the non-relativistic spectroscopic nomenclature of charmonium states [33], J/ψ ($\psi(3097)$) is ground state and $\psi(2S)$ ($\psi(3686)$) is its first excited state ([50], [51]). Charmonium states can also be produced in other processes like; B-decays ([52], [53]), two photon collision process [54], etc. Charmonium states that can not be produced directly in e^-e^+ annihilations, are obtained from radiative and hadronic transitions of their higher energy states e.g., radiative and hadronic transitions of $\psi(2S)$ can provide samples of lower energy charmonium companions. This technique of studying indirect charmonium states has been used by BES as well as CLEO Collaborations [55]. Fig. 4.2 shows directly and indirectly accessible charmonium.

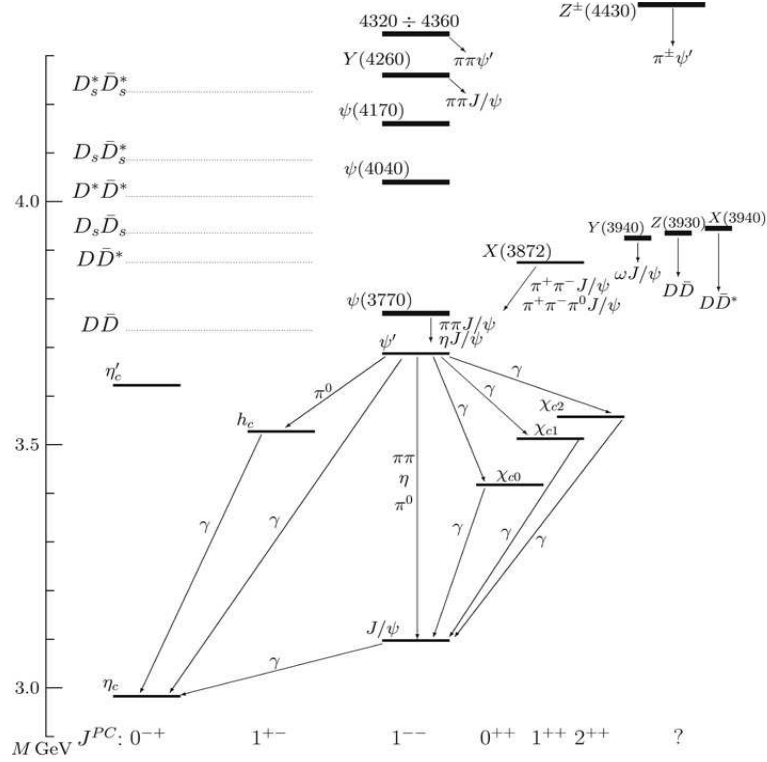


Figure 4.2: Known charmonium states and their radiative transitions: electromagnetic and hadronic. The dotted lines indicate threshold energy levels for charmonium decays into pairs of charmed mesons [50].

A charmonium system can be used to probe important aspects of electroweak and strong interactions, in different scenarios like; electromagnetic and hadronic transitions among charmonium states, annihilation decays of charmonium states into light hadrons and charmonium decays at or above open charm threshold ($D^0\bar{D}^0$ threshold) ([50], [51]). Charmonium investigation can provide detailed information about perturbative and non-perturbative regions of QCD. It is an ideal laboratory for making precision tests of predictions of lattice QCD and effective field theory ([56], [57], [58], [59]). The following subsections take up discussion on electromagnetic and hadronic transitions among charmonium states as well as annihilation decays of J/ψ and $\psi(2S)$

resonances to light hadrons. More details are available in [50] and the references therein.

4.2.1 Electromagnetic Transitions

An atom can emit or absorb photons of only specific wavelengths. Wavelengths of photons emitted (or absorbed) give rise to an energy spectrum which provides characteristics of atom. An electromagnetic transition can be better understood by considering Hydrogen atom, the simplest bound system of an electron and a proton. In this atom, electron can attain only specific allowed energy levels. These energy levels are possible through their transitions involving emission or absorption of photons with particular wavelengths. In analogy, a charmonium state can undergo transition to lower charmonium states by emitting a photon of specific energy. These are called electromagnetic transitions of a charmonium state such as $\psi(2S)$. Fig. 4.3 elaborates such transitions based on the data recorded by Crystal Ball detector at SPEAR ([60], [61]). At or above a certain threshold energy, charmonium states become capable of decaying into charmed and anticharmed mesons: $D^0\bar{D}^0$ and excited pairs. Such states can be found among charmonium states grouped with respect to their orbital angular momentum, as shown in Fig. 4.4 ([60], [62]).

4.2.2 Hadronic Transitions

Similar to electromagnetic transitions, hadronic transitions take place through interaction of charm quark or/and antiquark with gluons that hadronize into light mesons

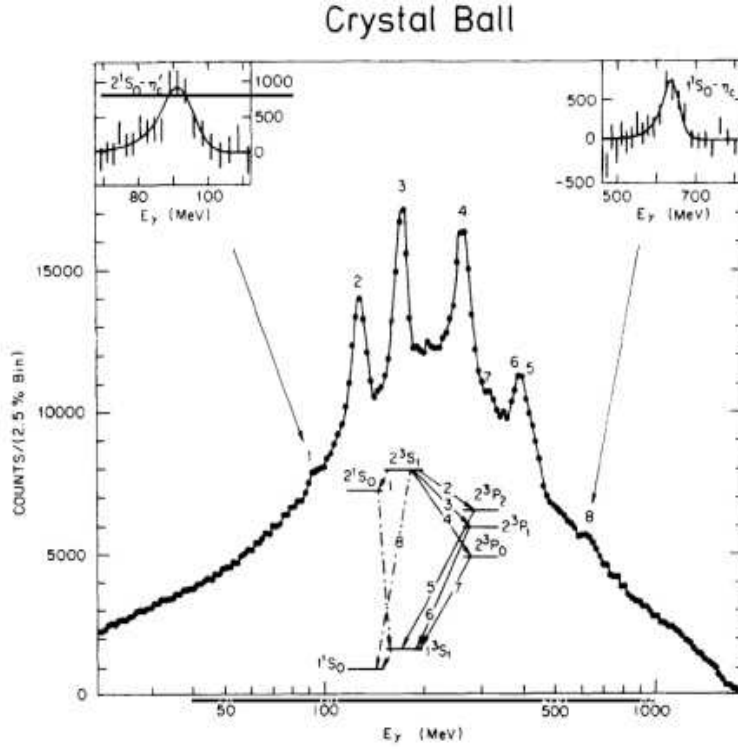


Figure 4.3: Electromagnetic decays of ψ family [61]

(e.g., pions and eta). For hadronic transitions, the interaction of a non-relativistic charmonium with the gluonic field can be described by using multipole expansion in QCD [63]. Due to color neutrality, physical hadronic transition amplitudes arise in at least second order interactions of the charm or/and anti-quark with the gluonic field. Fig. 4.2, in addition to electromagnetic transitions, also shows hadronic transitions.

4.2.3 Annihilation Decays

We will now take up the annihilation decays of J/ψ and $\psi(2S)$ charmonium resonances. According to perturbative QCD, the $c\bar{c}$ pair of these resonances has substantial probability to annihilate into three gluons or one photon (Fig. 4.5) followed by

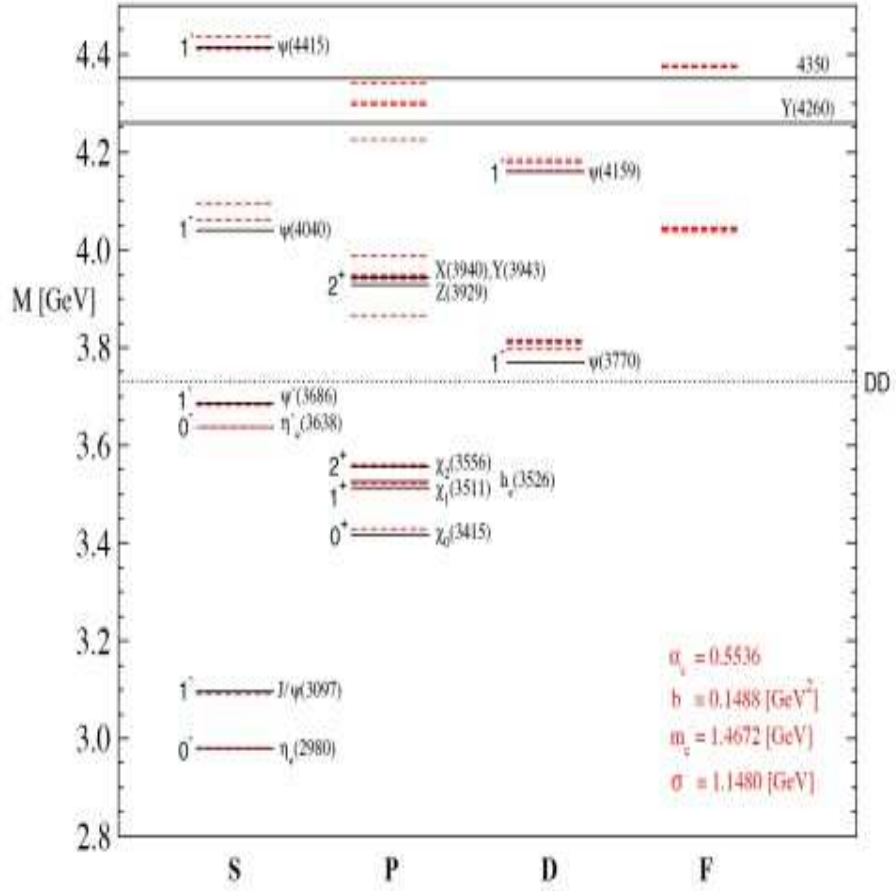


Figure 4.4: The XYZs of charmonium at BES [62]

lepton or hadron production [64].

The decays are highly suppressed by OZI rule as compared to the electromagnetic transitions. In this scenario, the annihilations can be placed in two categories: one through electromagnetic interaction and the other via strong interaction. The electromagnetic annihilation decays are allowed mainly through the annihilation of $c\bar{c}$ pair into a virtual photon leading to production of lepton pairs or light hadrons e.g $J/\psi \rightarrow \gamma^* \rightarrow X$ and $\psi(2S) \rightarrow \gamma^* \rightarrow X$. About 25% of J/ψ ([31], [50], [65], [66]), and

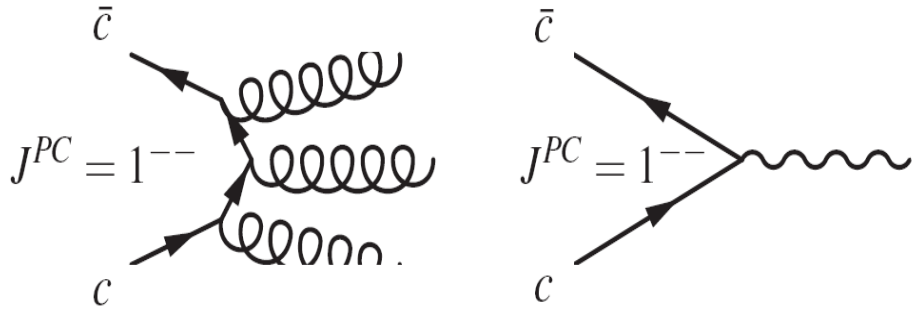


Figure 4.5: Charmonium annihilation decay through three gluons and one photon [38]

about 3.4% of $\psi(2S)$ ([50], [65]) decays take place through electromagnetic annihilations. The strong annihilations involve conversion of $c\bar{c}$ pair into minimal number of gluons i.e., three or more gluons. Annihilation to one gluon is prohibited due to non-conservation of color charge while annihilation to two gluons is forbidden by non-conservation of negative C parity [50]. The allowed gluon states subsequently lead to the production of specific hadronic states.

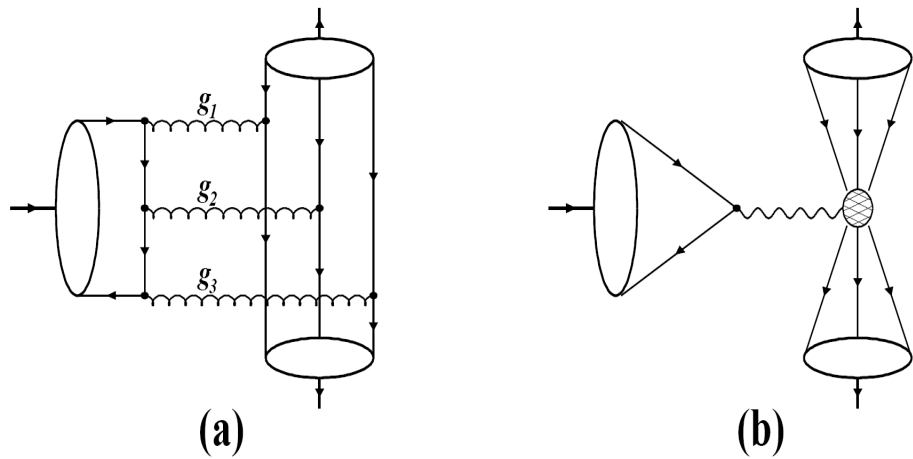


Figure 4.6: Feynman diagrams for charmonium annihilation decays: (a) strong annihilation decay to baryon antibaryon pair (b) electromagnetic annihilation decay to baryon anti-baryon pair [67].

The hadronic products produced provide us an opportunity to investigate 'the charmonium decays to baryon antibaryon ($B\bar{B}$) pairs' (Fig. 4.6). As argued by various authors, ([67], [68], [69], [70], [71]) the dominant mechanism in the production of $B\bar{B}$ pairs is the annihilation of $c\bar{c}$ pair into three gluons (the minimum number) that materialize into three light quark antiquark pairs. These light quark antiquark pairs hadronize into $B\bar{B}$ pair. This mechanism is well reflected in the narrow hadronic decay width of the charmonium states [72].

For baryon antibaryon pair thus produced, there exist possibilities: $B_8\bar{B}_8$ (baryon and antibaryon belonging to the octets), $B_{10}\bar{B}_{10}$ (baryon and antibaryon belonging to the decuplets), $B_8\bar{B}_{10}$ (baryon belonging to octet and antibaryon belonging to the decuplet) and $B_{10}\bar{B}_8$ (baryon belonging to decuplet and antibaryon belonging to the octet). Recently, results on $\psi(2S)$ decays into baryon antibaryon pairs, have been reported using 3.95×10^6 $\psi(2S)$ events recorded by BES I [73], 14×10^6 $\psi(2S)$ events recorded by BES II [74] and 3.08×10^6 $\psi(2S)$ events recorded by CLEO-c [75]. One of the possibilities in the measurements at these laboratories is the production of $\Omega^-\bar{\Omega}^+$ (a decuplet baryon antibaryon pair) which is the focus of our analysis. In the following section, we will briefly describe the main decay modes of Ω^- and $\bar{\Omega}^+$.

4.3 Non-Leptonic Decays of Ω^- and $\bar{\Omega}^+$

As nicely described by *Oleg Kamaev* [76] (and the references therein), we briefly overview the non-leptonic decay modes of Ω^- and $\bar{\Omega}^+$ as below:

The Ω^- baryon is composed of three strange quarks (sss) in a totally symmetric

flavor-spin-space state, whereas $\bar{\Omega}^+$ consists of three antistrange quarks ($\bar{s}\bar{s}\bar{s}$). They can decay only through weak interaction in which the strange quark (antistrange quark) flavor is changed into an up or down quark (antiup or antidown quark) flavor, giving Ω^- with an extremely long life time i.e., $\tau \sim 8 \times 10^{-11}s$, as compared to other hyperons in the decuplet [77]. Although the weak interaction is well understood, decay characteristics of strange quarks (antiquarks) making hadrons have not been sufficiently understood. In this regard, experimental measurements and theoretical calculations of the decay properties of Ω^- and $\bar{\Omega}^+$ are very helpful. In order to investigate as to how the weak decays of hyperons take place in the presence of strong force, study of non-leptonic decays of hyperons as stressed by D. Wu and J. L. Rosner [78], are essential.

The dominant decay modes of Ω^- and $\bar{\Omega}^+$ are: $\Omega^- \rightarrow \Lambda K^-$ and $\bar{\Omega}^+ \rightarrow \bar{\Lambda} K^+$, respectively, each of branching fraction $(67.8 \pm 0.7)\%$ [31]. The decay process: $\Omega^- \rightarrow \Lambda K^-$ takes place when a strange quark of Ω^- is changed into an up or a down quark. First of all, we see how the decay process proceeds forward through conversion of a strange quark into an up quark. In this case, a W^- gauge boson is emitted by a strange quark of Ω^- , that subsequently produces a quark antiquark pair: $d\bar{u}$. The antiquark: \bar{u} combines with one of the two strange quarks of Ω^- to form a K^- meson, and the down quark combines with remaining quarks: one strange and one up quark, to form Λ baryon. After the Λ baryon is formed, it predominantly decays into $p\pi^-$ with branching fraction of $((63.9 \pm 0.5)\%)$ [31], through conversion of its strange quark into an up quark. In this case the emitted gauge boson: W^- , again produces a quark

antiquark pair: $d\bar{u}$. Subsequently, according to the requirement of color neutrality of hadrons, a proton $p(uud)$ and a pion $\pi^- (d\bar{u})$ are produced, thus giving proton p , kaon K^- and pion π^- as the final decay products of Ω^- . The antibaryon: $\bar{\Omega}^+$, decays on the same lines, to the final state comprising antiproton \bar{p} , kaon K^+ and pion π^+ , through change of antistrange quark into antiup quark. Secondly, a strange quark is changed into a down quark. In this case, strange quark first transforms into intermediate quark state: charm, bottom or top, by emitting W^- gauge boson. The intermediate quark radiates a gluon that materializes into a $u\bar{u}$ pair. The intermediate quark subsequently absorbs the emitted W^- gauge boson and transforms into a down quark. The color neutral combination of three quarks (uds) forms the Λ baryon and the colorless combination of a quark-antiquark pair: $s\bar{u}$ produces kaon: K^- . The decay of Λ , through change of strange quark into down quark, takes place in the same way. The weak processes involved in changing strange quark into up or down quark, are shown as Feynman diagrams in Fig. 4.7.

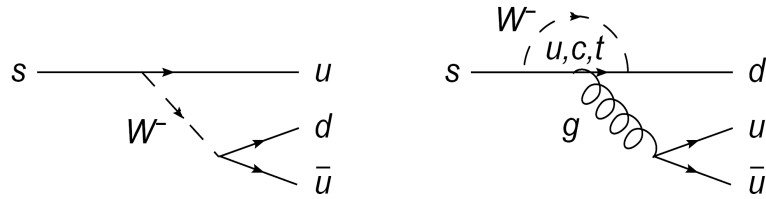


Figure 4.7: The left diagram (Tree-level diagram) represents change of strange quark flavor into an up quark flavor and the diagram on the right (Penguin diagram) shows how a strange quark flavor is changed into a down quark flavor [76]

In addition to the dominant decay mode: $\Omega^- \rightarrow \Lambda K^-$ and $\bar{\Omega}^+ \rightarrow \bar{\Lambda} K^+$, there are rare non-leptonic decay modes including: $\Omega^- \rightarrow \Xi_{1530}^{*-} \pi^0$, $\Omega^- \rightarrow \Xi_{1530}^{*0} \pi^-$, $\Omega^- \rightarrow \Xi^- \pi^+ \pi^-$,

$\Omega^- \rightarrow \Xi^- \pi^0 \pi^-$, $\Omega^- \rightarrow \Xi^- \pi^0 \pi^0$, etc, along with similar conjugate decay modes. These decay modes have very small branching fractions, thus providing only small data samples. The dominant decay mode and the rare non-leptonic decay modes are the first order weak decays, because only one strange quark is converted into an up or a down quark. The second order weak decays of Ω^- and $\bar{\Omega}^+$, such as $\Omega^- \rightarrow \Lambda \pi^-$ and $\bar{\Omega}^+ \rightarrow \bar{\Lambda} \pi^+$, are predicted to have very small branching fractions within the Standard Model. For example the predicted branching fraction for $\Omega^- \rightarrow \Lambda \pi^-$ is of the order of 10^{-17} [79], consistent with the recent upper limit: $B(\Omega^- \rightarrow \Lambda \pi^-) \leq 2.9 \times 10^{-6}$ obtained using data of HyperCP experiment [80].

Search for Ω^- and $\bar{\Omega}^+$ in $\psi(2S)$ decay products is therefore a challenging task in view of very low probability of $\psi(2S) \rightarrow \Omega^- \bar{\Omega}^+$ process. In the next section, we will encounter the efforts made in this regard.

4.4 Search for Ω^- and $\bar{\Omega}^+$ in $\psi(2S)$ Decays

We described earlier that the dominant decay modes of Ω^- and $\bar{\Omega}^+$ are $\Omega^- \rightarrow \Lambda K^-$ and $\bar{\Omega}^+ \rightarrow \bar{\Lambda} K^+$, respectively. It is therefore favorable to look for Ω^- and $\bar{\Omega}^+$ hadrons in $\psi(2S)$ decay products through these decay modes. The upper limits for $\psi(2S) \rightarrow \Omega^- \bar{\Omega}^+$, at 90% confidence level have been reported by BESII [73] and CLEO-c [75], Collaborations. The BESII result was based on 3.95×10^6 $\psi(2S)$ recorded decay events. In this work, the dominant decay chains: $\Omega^- \rightarrow \Lambda K^-$, $\Lambda \rightarrow p \pi^-$ and $\bar{\Omega}^+ \rightarrow \bar{\Lambda} K^+$, $\bar{\Lambda} \rightarrow \bar{p} \pi^+$ were used, reporting an upper limit of 7.3×10^{-5} at 90% confidence level. Fig. 4.8 shows the invariant mass of ΛK^- , for both the MC as well

as the data events, left after all selection criteria. The Monte-Carlo events were normalized to the data events obtained. The histogram bars represent the data whereas crosses represent the MC candidate events. It is obvious from this figure that there are no data events within 3σ of the central mass value of Ω^- i.e., $1.672 \text{ GeV}/c^2$ [31]. The second upper limit result, by CLEO Collaboration, was based upon a study of 3.08×10^6 $\psi(2S)$ decays [81]. This study also used the dominant decay chains of Ω^- and $\bar{\Omega}^+$, giving an upper limit of 1.6×10^{-4} , at 90% confidence level. The invariant mass distribution of ΛK^- is shown in Fig. 4.9. BESII result for $B(\psi(2S) \rightarrow \Omega^- \bar{\Omega}^+)$ was an improvement over the measurement of CLEO-c.

In order to search for Ω^- and $\bar{\Omega}^+$ in $\psi(2S)$ decay events, we have performed a detailed analysis based upon 14 million $\psi(2S)$ decay events recorded by BESII detector. Details of our analysis, based on novel technique of selecting events with one missing charge track also and used for the first time, are given in the next chapter.

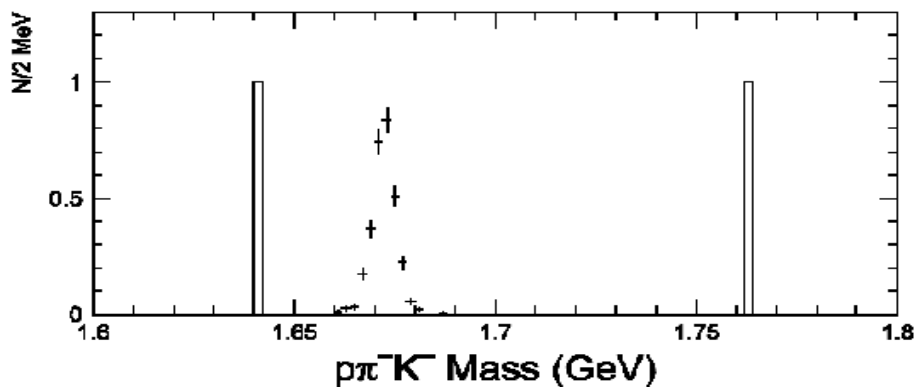


Figure 4.8: BES Result: $Br(\psi(2S) \rightarrow \Omega^- \bar{\Omega}^+) \leq 7.3 \times 10^{-5}$ at 90% confidence level. The crosses represent the MC invariant mass distribution of ΛK^- normalized to the data events. Within 3σ signal region there are no data signal events [73].

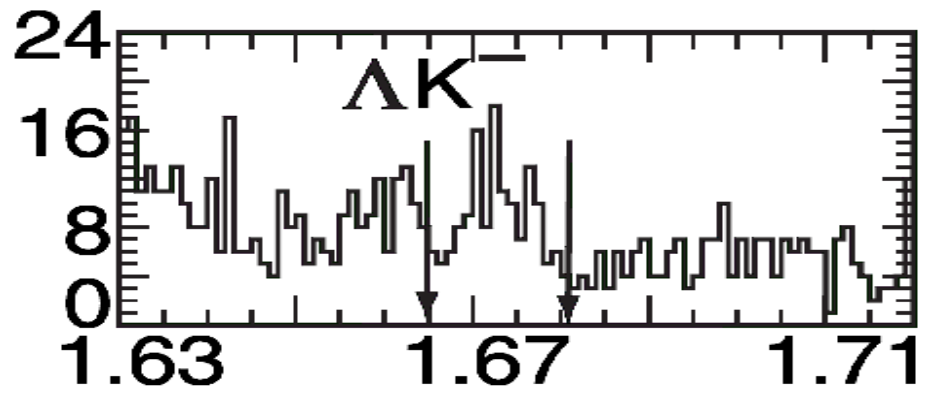


Figure 4.9: CLEO Result: $Br(\psi(2S) \rightarrow \Omega^- \bar{\Omega}^+) \leq 1.6 \times 10^{-4}$ at 90% confidence level. Here, the invariant mass distribution of ΛK^- is only from data events [75].

Chapter 5

STUDY OF $\psi(2S) \rightarrow \Omega^- \bar{\Omega}^+$

5.1 Introduction

¹The production of $\psi(2S)$ in e^+e^- annihilation and its two body hadronic decays can be used to test the predictive power of QCD [84]. As described above, $\psi(2S)$ predominantly decays either through $c\bar{c}$ annihilation into three gluons or a photon. Gluons or photon leads to the hadron production. The hadrons produced may be baryon antibaryon pair such as $\Omega^- \bar{\Omega}^+$. The decay process $\psi(2S) \rightarrow \Omega^- \bar{\Omega}^+$ is a special case in which Ω^- and $\bar{\Omega}^+$ are predominantly produced from materialization of three gluons or a photon into three $s\bar{s}$ quark antiquark pairs. Three s quarks make up Ω^- baryon whereas three \bar{s} anti-quarks form $\bar{\Omega}^+$. The earlier studies of this decay channel; [73] and [74] have reported upper limits for its branching fraction,

¹This chapter is based on our BESII analysis memo and draft paper, both titled *First Evidence of $\psi(2S) \rightarrow \Omega^- \bar{\Omega}^+$* , submitted to the BES Collaboration ([82], [83]). Similarity in the text, figures and tables, with our analysis memo and draft paper is therefore inevitable. The analysis memo and draft paper are available at BES publication page (bes.ihep.ac.cn, with restricted access).

at 90% confidence level. The particles in the final state of $\psi(2S) \rightarrow \Omega^-\bar{\Omega}^+$, have low momentum values ($p < 0.8 \text{ GeV}/c$). Therefore the possibility of missing particle track from the final state, increases. Taking into account this factor, we have used a new approach to analyze this decay process by additionally using the concept of one missing particle/track from the final state. In case of all 6 particles present in the final state, the detection efficiency is found to be 1.7% whereas for 6 particles or 5 particles in the final state, the detection efficiency is found to be 8.3%. From our study we obtain first evidence of Ω^- and $\bar{\Omega}^+$ signals with statistical significance levels of 5.3σ and 4.6σ respectively. The branching fraction is first time determined to be $(3.21 \pm 1.25(stat) \pm 0.97(sys)) \times 10^{-5}$.

5.2 Monte-Carlo And Data Samples

The signal channel ($\psi(2S) \rightarrow \Omega^-\bar{\Omega}^+$) was studied by using the following MC and data samples:

1. A sample of 10^5 inclusive MC events of $\psi(2S) \rightarrow \Omega^-\bar{\Omega}^+$, was generated by using 'P2BB event generator' [85] with a nominal value for angular distribution parameter: $\alpha = 0$. The events were generated such that Ω^- and $\bar{\Omega}^+$ decay into different final states, according to their relevant branching fractions available in Particle Data Group (PDG) [31].
2. Detector simulation of the events thus generated was performed using SIMBES V10403 program based upon GEANT3 [47]. The simulated data thus obtained

was saved in the form of a RAW file.

3. Subsequently, the data saved was reconstructed to get useful information about the MC events, in the form of an NDST file.
4. An event selection program written in FORTRAN language, was used to select the signal events from NDST file. The events thus selected were used to determine the detection efficiency and mass resolution for the signal channel.
5. A set of NDST files containing 14 million $\psi(2S)$ data was used to select candidate events for the signal channel.
6. Background analysis was performed using; a sample of 14 million $\psi(2S)$ inclusive MC sample generated by Lund-Charm generator developed at BES ([86], [87]) and exclusive MC samples for different decay processes.
7. Several other MC samples and data samples (such as J/ψ sample) were used for systematic error analysis.

The analysis details are provided in the next sections.

5.3 Initial Event Selection

The momentum values of final state particles in $\psi(2S) \rightarrow \Omega^- \bar{\Omega}^+$ lie below 0.8 GeV/c. Tracks of particles lying in the low momentum range may not be reconstructed by the detector. Thus, there is a large probability of missing particle tracks from the final state. Taking into account this factor, we employed a new technique of selecting

events with one missing track also.

Tracks of all selected events (including those with one missing track) were required to satisfy the following criteria:

- The tracks reconstructed from MDC should have good helix fit; MFIT=2.
- Polar angle of each charge track inside MDC, satisfies $|\cos\theta| \leq 0.8$.
- Each track is required to have transverse momentum of 0.07 GeV/c at the minimum i.e., $P_{xy} \geq 0.07$ GeV/c.
- The total momentum of each track satisfies $p \leq 1.2$ GeV/c.
- The number of charge tracks of an event satisfying above conditions (called good charge tracks), is required to be 6 or 5.
- Net charge is required to be 0 (for 6 good charge tracks) and +1 or -1 (for 5 good charge tracks).
- The point of closest approach to the interaction region, for each track, should satisfy the inequalities; $Rxy = \sqrt{x_0^2 + y_0^2} \leq 0.2$ m and $|z_0| \leq 0.3$ m, where x_0 , y_0 and z_0 are the coordinates of the point of closest approach to the interaction point.

5.4 Particle Identification

Each track of an event represents certain type of particle. Therefore all tracks of an event passing successfully the above selection criteria, were passed through the process

of particle identification. As particles in the final state of signal channel ($\psi(2S) \rightarrow \Omega^- \bar{\Omega}^+$) have low momentum values ($p < 0.8$ GeV/c), only ionization energy loss (dE/dx) information of tracks was considered more suitable for particle identification. This is because for both dE/dx and TOF information, detection efficiency was found to decrease. The dE/dx information was used to determine χ^2 values for each of the particle hypotheses (p, π^+, K^+ or \bar{p}, π^-, K^-):

$$\chi_{dE/dx}^2(i) = \left[\frac{dE/dx_{meas} - dE/dx_{exp}(i)}{\sigma_{dE/dx}(i)} \right]^2,$$

where dE/dx_{meas} , $dE/dx_{exp}(i)$ and $\sigma_{dE/dx}(i)$ represent measured dE/dx , expected dE/dx and dE/dx resolution for a particle hypothesis i , respectively. A particle hypothesis was assigned to a track if the $\chi_{dE/dx}^2$ value satisfies one of the following inequalities:

- Proton (p) hypothesis:

$$\chi_{dE/dx}^2(p) < \chi_{dE/dx}^2(\pi^+) \ \&\& \ \chi_{dE/dx}^2(p) < \chi_{dE/dx}^2(K^+)$$

- Positive pion (π^+) hypothesis:

$$\chi_{dE/dx}^2(\pi^+) < \chi_{dE/dx}^2(p) \ \&\& \ \chi_{dE/dx}^2(\pi^+) < \chi_{dE/dx}^2(K^+)$$

- Positive kaon (K^+) hypothesis:

$$\chi_{dE/dx}^2(K^+) < \chi_{dE/dx}^2(\pi^+) \ \&\& \ \chi_{dE/dx}^2(K^+) < \chi_{dE/dx}^2(p).$$

Hypotheses for negative charge tracks were decided based on similar criteria.

5.5 Kinematic Fitting

After particle identification, an event with 6 or 5 identified particle hypotheses was accepted for further processing. For an event with 6 particle hypotheses ($N_p = 1$, $N_{\bar{p}} = 1$, $N_{\pi^-} = 1$, $N_{\pi^+} = 1$, $N_{K^-} = 1$, $N_{K^+} = 1$ and thus $N_{total} = 6$), a four-constraint (4C) kinematic fit was applied imposing conservation of total energy and momentum. An event with 5 particle hypotheses ($N_p \leq 1$, $N_{\bar{p}} \leq 1$, $N_{\pi^-} \leq$

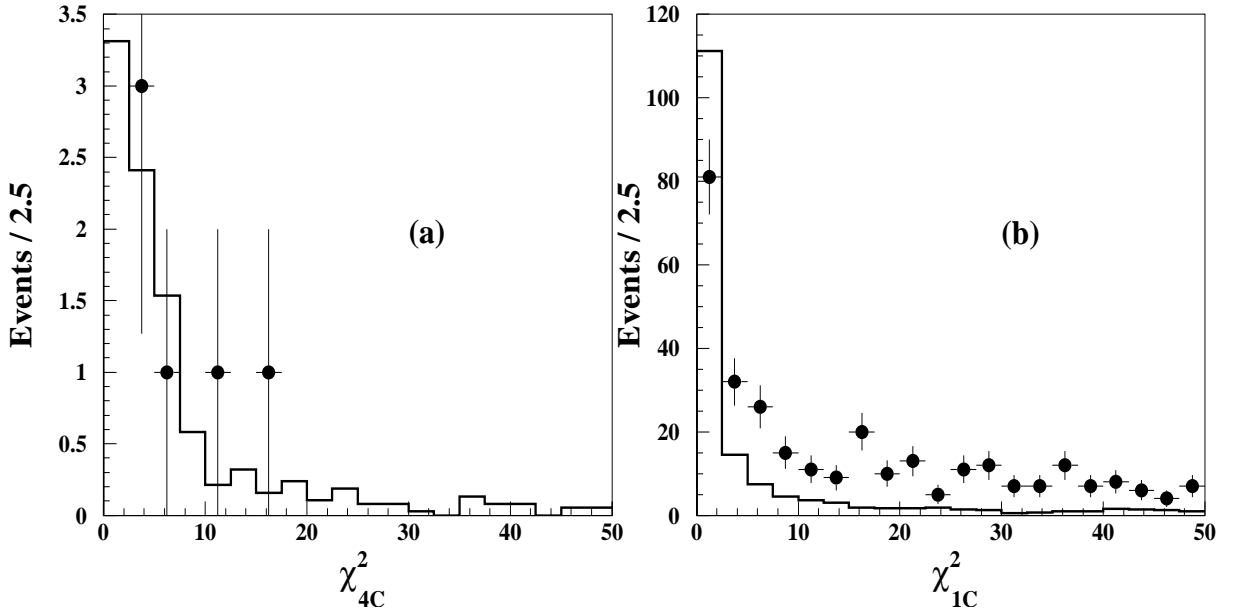


Figure 5.1: The χ^2 distributions [82]: (a) χ^2_{4C} distribution: the histogram is for MC and the dots with error bars represent data events passing successfully through 4C kinematic fit (b) χ^2_{1C} distribution: the histogram is for MC and the dots with error bars represent data events obtained after 1C kinematic fit.

1, $N_{\pi^+} \leq 1$, $N_{K^-} \leq 1$, $N_{K^+} \leq 1$ and $N_{total} = 5$), was subjected to a one-constraint (1C) kinematic fit imposing total energy conservation, under one of the hypotheses about the final state particles: $p\bar{p}\pi^+\pi^-K^+$ (K^- missing), $p\bar{p}\pi^+\pi^-$ (K^+ missing) K^- , $p\bar{p}\pi^+$ (π^- missing) K^+K^- , $p\bar{p}$ (π^+ missing) $\pi^-K^+K^-$, p (\bar{p} missing) $\pi^+\pi^-K^+K^-$ and

(p missing) $\bar{p}\pi^+\pi^-K^+K^-$. Important information about the event passing 4C or 1C kinematic fit, was obtained in the form of χ^2 distribution of kinematic fit, momentum distributions of final state particles & their parent resonances and invariant mass spectra for primary and intermediate resonances etc. The Λ , $\bar{\Lambda}$, Ω^- and $\bar{\Omega}^+$ resonances were investigated by using invariant mass spectra: $M(p\pi^-)$, $M(\bar{p}\pi^+)$, $M(\Lambda K^-)$ and $M(\bar{\Lambda}K^+)$, respectively. All the signal MC and data events were subjected to kinematic fit to obtain samples of events for final selection. A comparison between MC and data χ^2 distributions (from 4C and 1C kinematic fits) is shown in Fig. 5.1. These distributions seem not very well consistent with each other, because χ^2 distributions of data represent both the signal as well as background events whereas χ^2 distributions of MC represent only the signal events.

The momentum distributions of final state particles for signal MC are shown in Fig. 5.2. These distributions indicate that the momentum values of final state particles of the signal channel: $\psi(2S) \rightarrow \Omega^-\bar{\Omega}^+$, lie below 0.8 GeV/c. The momentum values of π^+ and π^- lie below 0.4 GeV/c and those of K^+ and K^- can be seen lying below 0.6 GeV/c. The proton and antiproton have comparatively larger momentum values, below 0.8 GeV/c. As described in section 3.2.3, BESII detector has good performance in π/K separation (below 600 MeV/c) and p/K separation (below 900 MeV/c), by using dE/dx information. Therefore, in our case, using only dE/dx information for particle identification, is not bad. Using sets of MC and data events obtained from kinematic fit, we reconstructed important invariant mass spectra including those of $p\pi^-$, $\bar{p}\pi^+$, ΛK^- and $\bar{\Lambda}K^+$. These mass spectra are shown in Fig. 5.3 to Fig. 5.6.

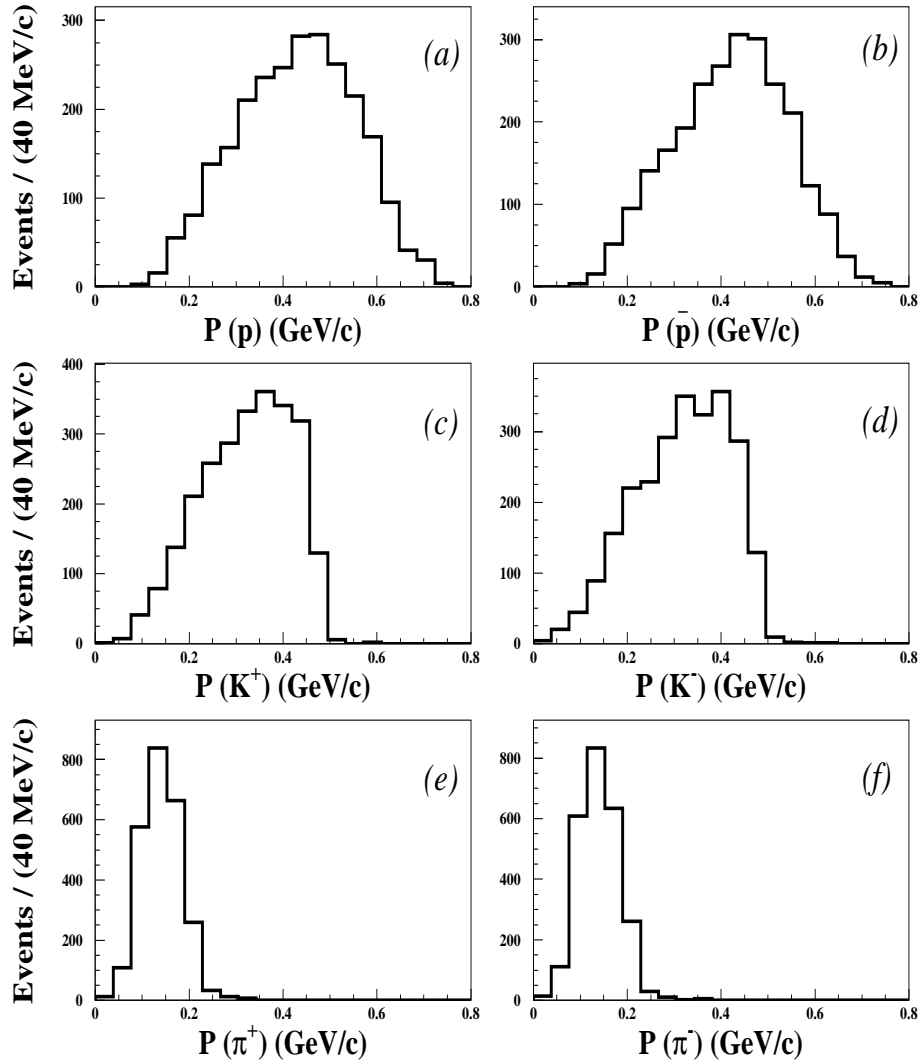


Figure 5.2: Momentum distributions (GeV/c) of final state particles: (a) proton (p) (b) antiproton (\bar{p}) (c) kaon (K^+) (d) kaon (k^-) (e) pion (π^+) and pion (π^-), of MC signal events passing successfully 4C or 1C kinematic fits, without any mass or χ^2 constraints [83].

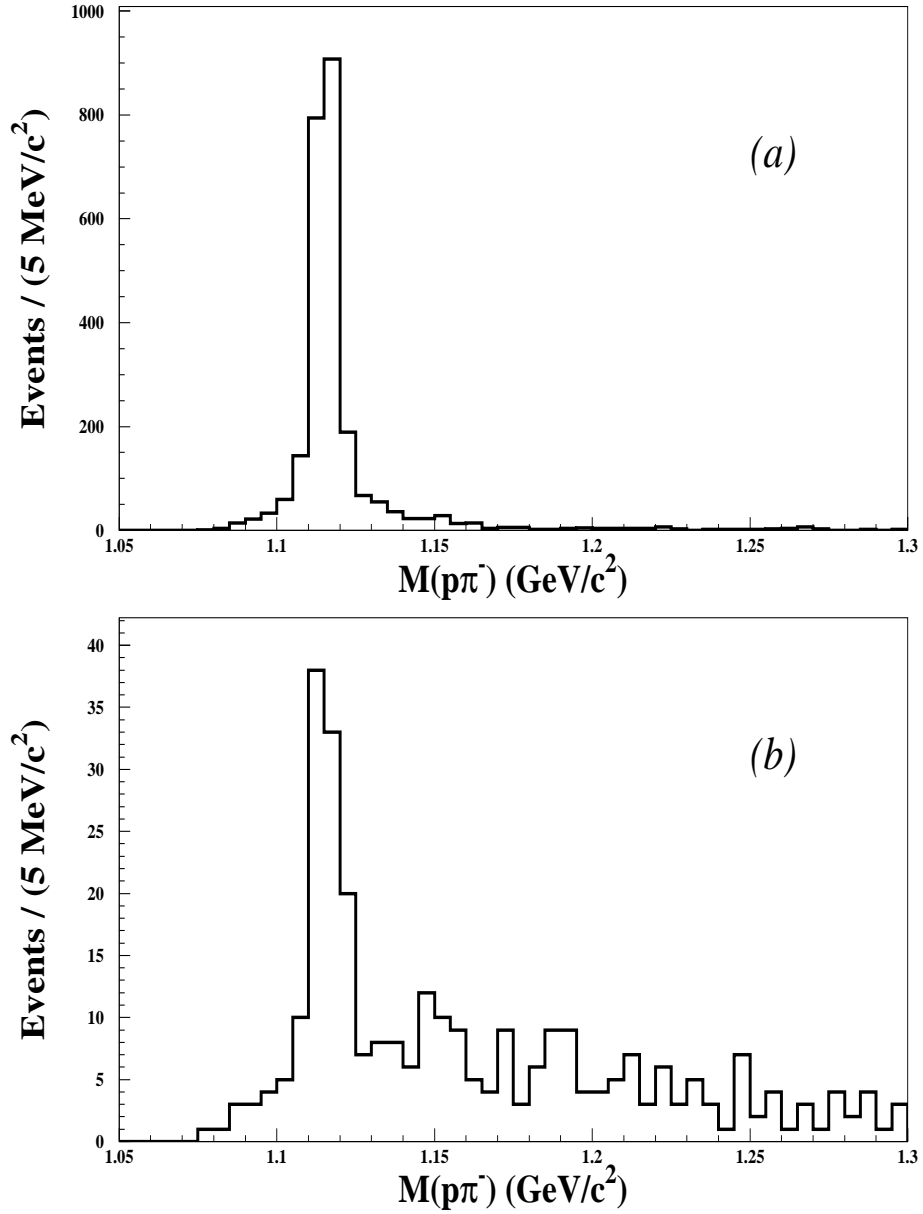


Figure 5.3: Invariant mass spectra of $p\pi^-$ (GeV/c^2) reconstructed by using four momenta of proton (p) and pion (π^-) belonging to the events passing 4C or 1C kinematic fit: (a) $M(p\pi^-)$ for MC events and (b) $M(p\pi^-)$ for data events, without any mass or χ^2 constraints [83].

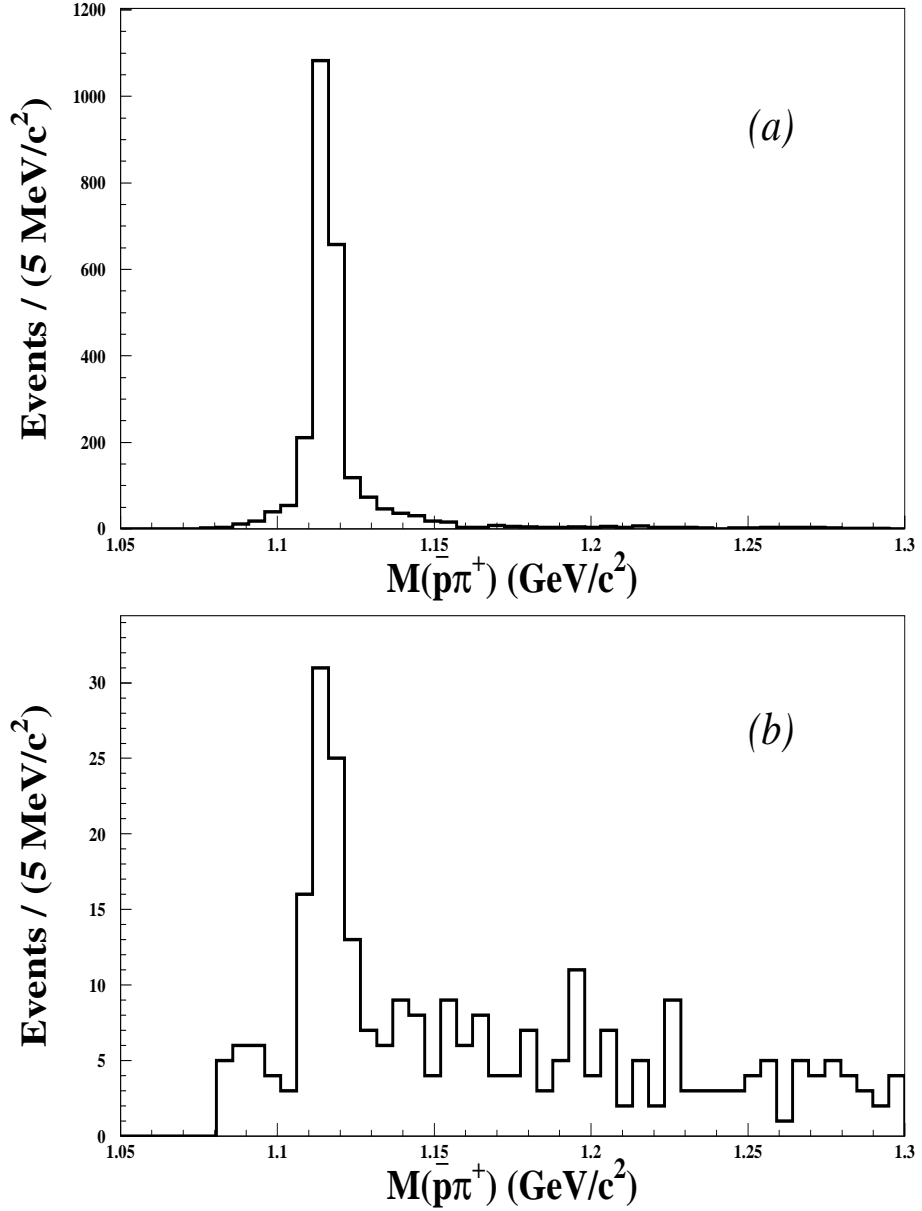


Figure 5.4: $\bar{p}\pi^+$ invariant mass spectra (GeV/c^2) reconstructed from four momenta of antiproton (\bar{p}) and pion (π^+) belonging to the events obtained from 4C or 1C kinematic fit: (a) from signal MC and (b) from data, without any mass or χ^2 constraints [83].

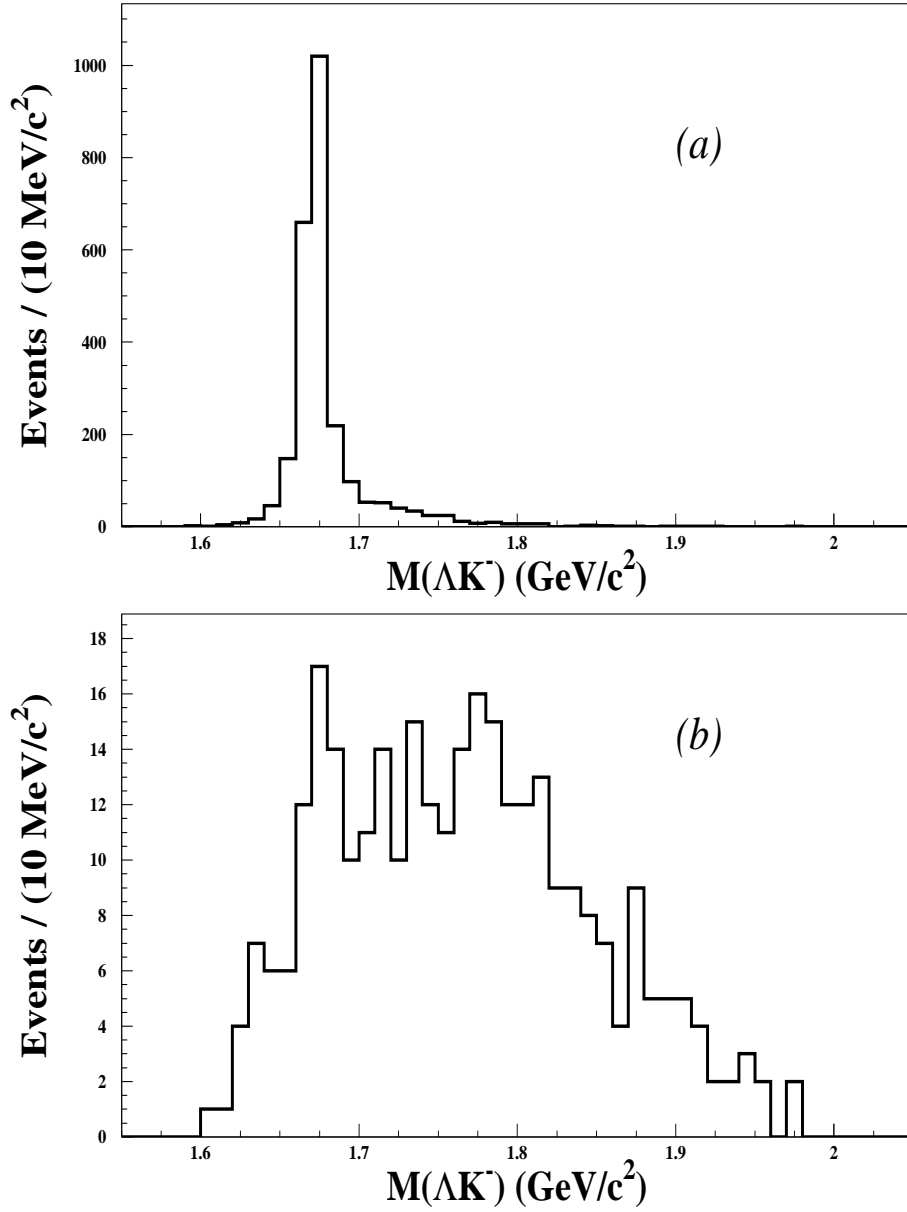


Figure 5.5: ΛK^- invariant mass spectra (GeV/c^2) obtained by using four momenta of reconstructed Λ and K^- for events passing 4C or 1C kinematic fit: (a) from signal MC and (b) from data, without any mass or χ^2 constraints [83].

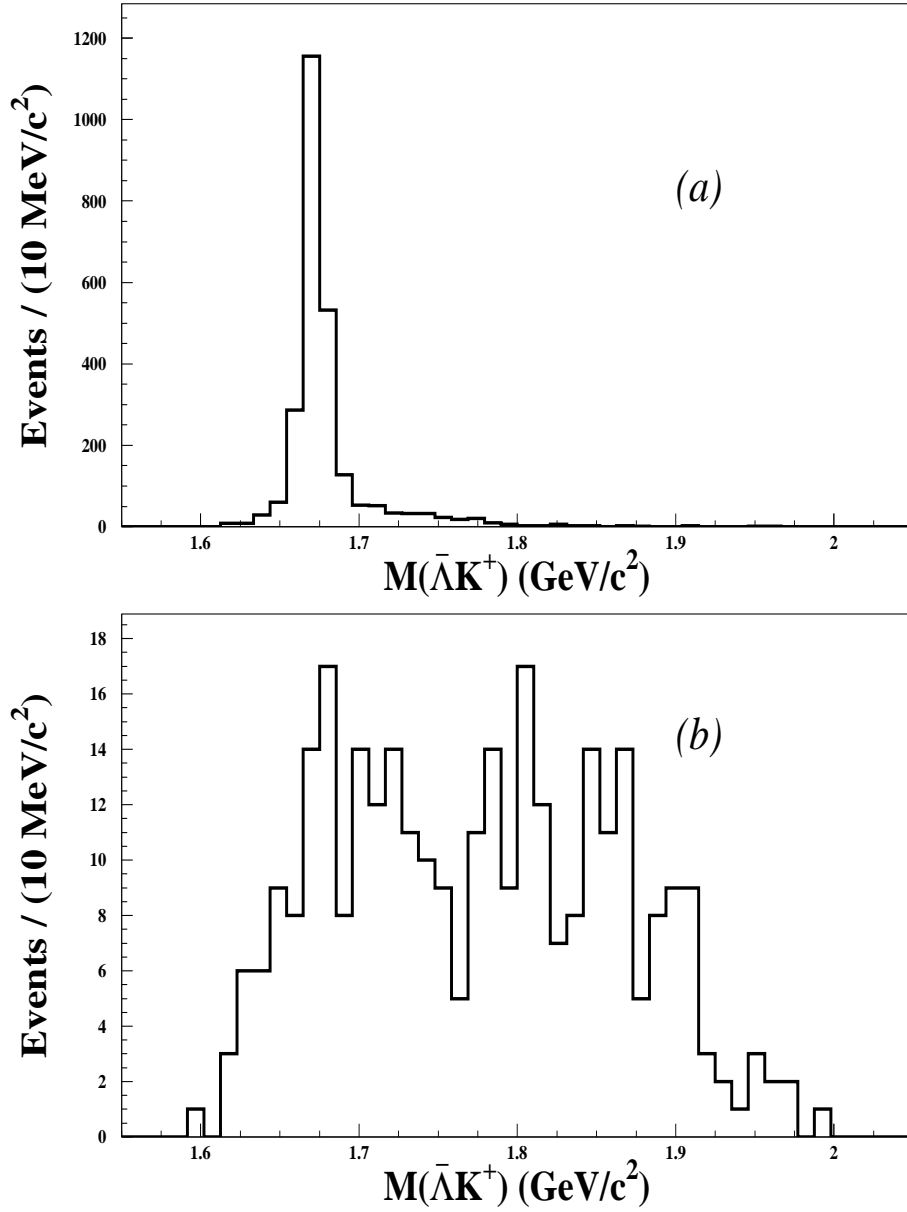


Figure 5.6: $\bar{\Lambda}K^+$ invariant mass spectra (GeV/c^2) obtained by using four momenta of reconstructed $\bar{\Lambda}$ and K^+ for events passing 4C or 1C kinematic fit: (a) from signal MC and (b) from data, without any mass or χ^2 constraints [83].

5.6 Determination of $\Lambda(\bar{\Lambda})$ and $\Omega^-(\bar{\Omega}^+)$ Mass Resolutions

The mass resolutions (σ) of $\Lambda(\bar{\Lambda})$ and $\Omega^-(\bar{\Omega}^+)$ were estimated by making single gaussian fits to the peaks of relevant invariant mass spectra obtained from signal MC. The mass resolutions approximated are $0.004 \text{ GeV}/c^2$ and $0.0085 \text{ GeV}/c^2$, for $\Lambda(\bar{\Lambda})$ and $\Omega^-(\bar{\Omega}^+)$, respectively. The mass resolutions were used for deciding mass limits for $\Lambda(\bar{\Lambda})$ and $\Omega^-(\bar{\Omega}^+)$. The detail about the mass limits will be provided in section 5.8, as a part of criteria for final event selection.

5.7 Optimization of χ_{1C}^2

From 4C or 1C kinematic fit we obtained a sample of 309 data events. Only 6 events were obtained from 4C kinematic fit (all having $\chi_{4C}^2 < 20$). Remaining 303 events were obtained from 1C kinematic fit with χ_{1C}^2 ranging from 0 to 50. Due to low statistics of data events obtained from 4C fit, $\chi_{4C}^2 < 20$ was selected as a part of final selection criteria. χ_{1C}^2 was optimized for maximum value of $\frac{S}{\sqrt{S+B}}$, where S and $S+B$ represent the signal and signal plus background, respectively. A cut of $\chi_{1C}^2 < 10.0$ (Fig. 5.7) was decided to be used in final event selection.

5.8 Final Event Selection

In addition to $\chi_{4C}^2 < 20$ and $\chi_{1C}^2 < 10$ constraints, mass cuts were decided for final selection of events. The mass constraints of about 3σ from the central mass values, were used as a part of final selection criteria. $\chi_{4C}^2 < 20$ was used for events obtained through 4C kinematic fit whereas $\chi_{1C}^2 < 10$ was applied for events coming from 1C kinematic fit. The criteria for final selection of invariant mass spectra: $M(p\pi^-)$,

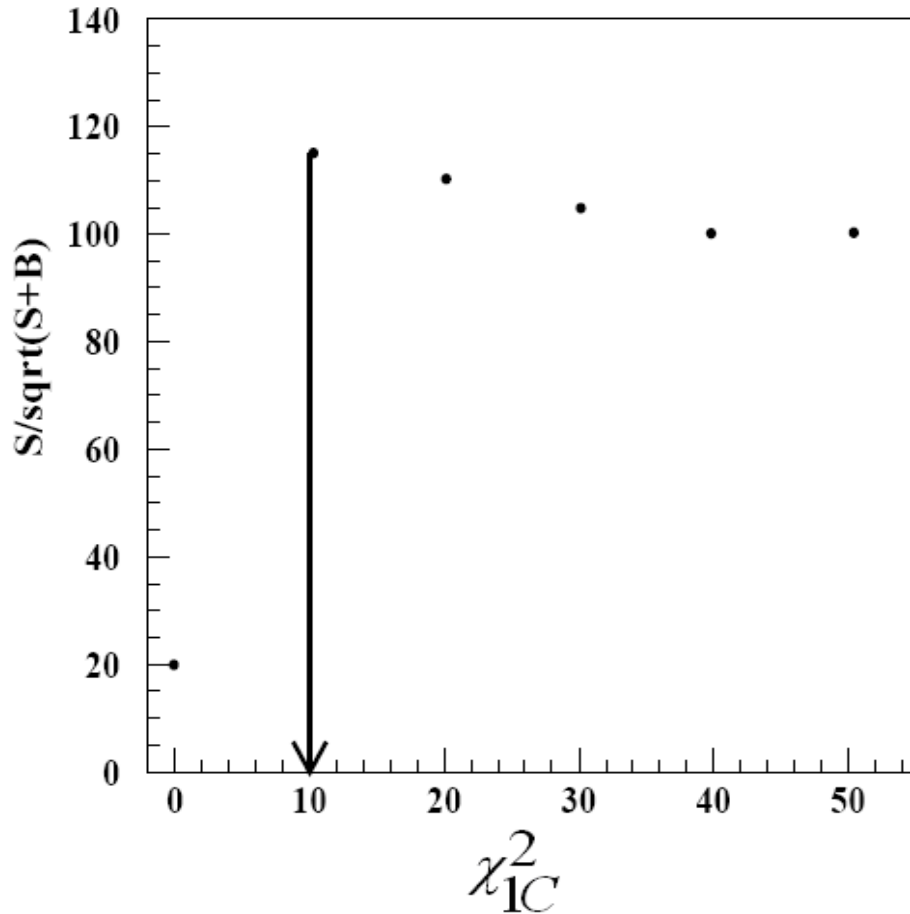


Figure 5.7: Optimization of χ_{1C}^2 : S represents the signal events whereas S+B represents signal plus background events. That χ_{1C}^2 cut is decided which optimizes the ratio: $S/\sqrt{S+B}$. In this way, the optimized cut is chosen to be $\chi_{1C}^2 < 10$ [83].

$M(\bar{p}\pi^+)$, $M(\Lambda K^-)$ and $M(\bar{\Lambda}K^+)$, is given as:

- The $p\pi^-$ invariant mass spectrum was obtained under following constraints:
 1. $\chi_{4C}^2 < 20$ or $\chi_{1C}^2 < 10$
 2. $|M_{\bar{p}\pi^+} - M_{\bar{\Lambda}}| < 0.012 \text{ GeV}/c^2$, where $M_{\bar{\Lambda}} = 1.115683 \text{ GeV}/c^2$
- The $\bar{p}\pi^+$ invariant mass distribution was obtained under following constraints:
 1. $\chi_{4C}^2 < 20$ or $\chi_{1C}^2 < 10$
 2. $|M_{p\pi^-} - M_{\Lambda}| < 0.012 \text{ GeV}/c^2$, where $M_{\Lambda} = 1.115683 \text{ GeV}/c^2$
- Invariant mass distribution of ΛK^- was obtained under following criteria:
 1. $\chi_{4C}^2 < 20$ or $\chi_{1C}^2 < 10$
 2. $|M_{p\pi^-} - M_{\Lambda}| < 0.012 \text{ GeV}/c^2$
 3. $|M_{\bar{p}\pi^+} - M_{\bar{\Lambda}}| < 0.012 \text{ GeV}/c^2$
 4. $|M_{\bar{\Lambda}K^+} - M_{\bar{\Omega}^+}| < 0.025 \text{ GeV}/c^2$, where $M_{\bar{\Omega}^+} = 1.672 \text{ GeV}/c^2$
- For $\bar{\Lambda}K^+$ invariant mass distribution, the following constraints were imposed:
 1. $\chi_{4C}^2 < 20$ or $\chi_{1C}^2 < 10$
 2. $|M_{p\pi^-} - M_{\Lambda}| < 0.012 \text{ GeV}/c^2$
 3. $|M_{\bar{p}\pi^+} - M_{\bar{\Lambda}}| < 0.012 \text{ GeV}/c^2$
 4. $|M_{\Lambda K^-} - M_{\Omega^-}| < 0.025 \text{ GeV}/c^2$, where $M_{\Omega^-} = 1.672 \text{ GeV}/c^2$

The invariant mass distributions thus obtained are shown in Fig. 5.8 to Fig. 5.11.

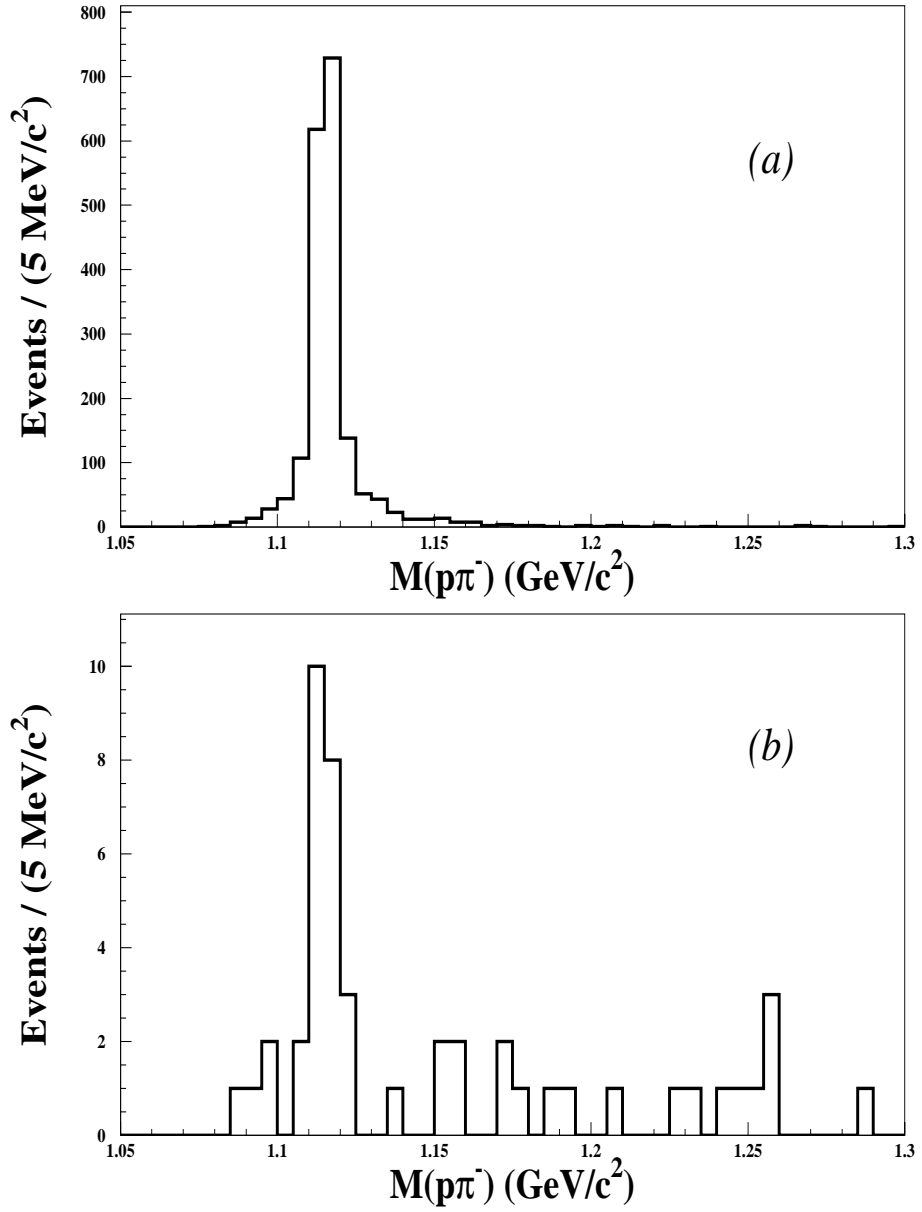


Figure 5.8: $p\pi^-$ invariant mass distributions: (a) from signal MC and (b) from data, under the constraints: $|M_{\bar{p}\pi^+} - M_{\bar{\Lambda}}| < 0.012 \text{ GeV}/c^2$ and $(\chi_{4C}^2 < 20$ or $\chi_{1C}^2 < 10)$ [83].

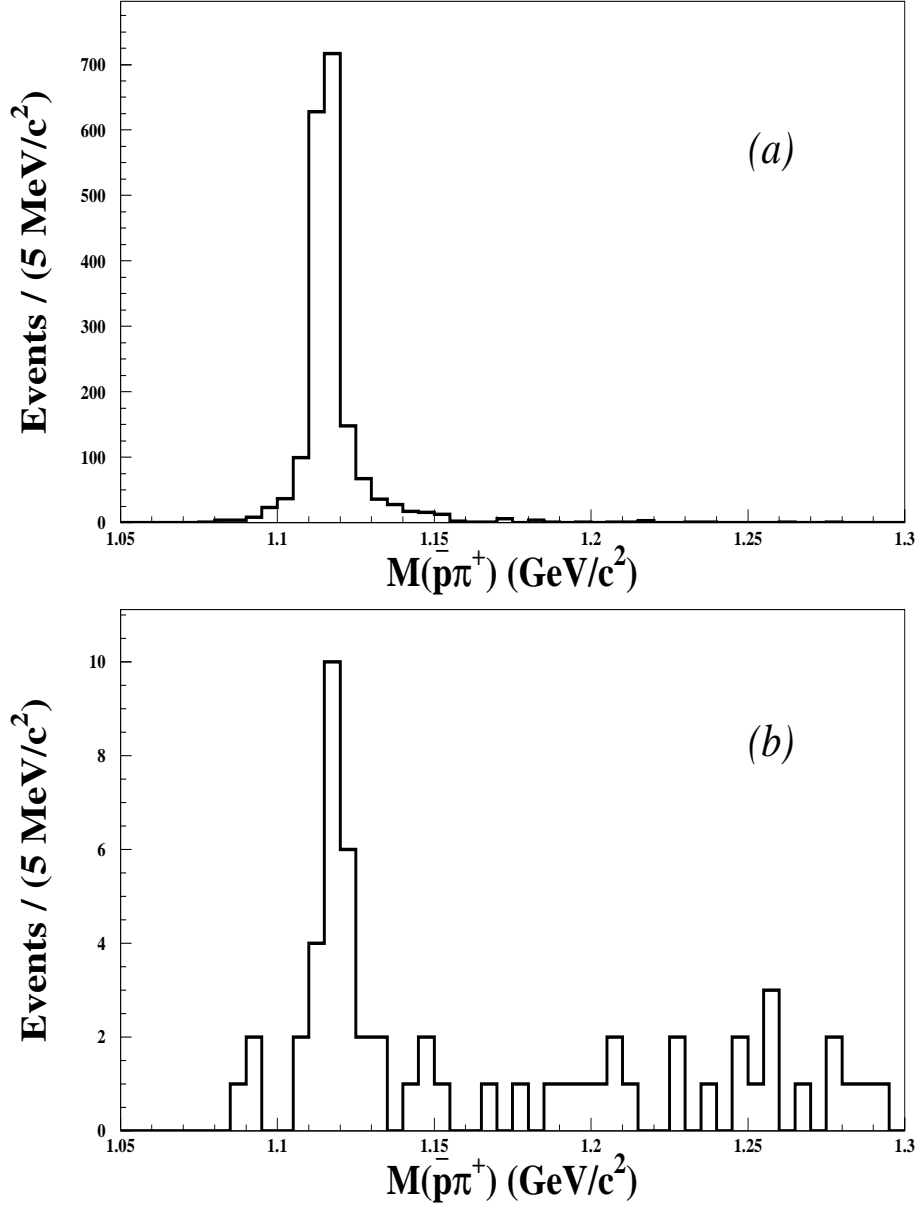


Figure 5.9: $\bar{p}\pi^+$ invariant mass plots: (a) from signal MC and (b) from data, under the constraints: $|M_{p\pi^-} - M_\Lambda| < 0.012 \text{ GeV}/c^2$ and $(\chi_{4C}^2 < 20 \text{ or } \chi_{1C}^2 < 10)$ [83].

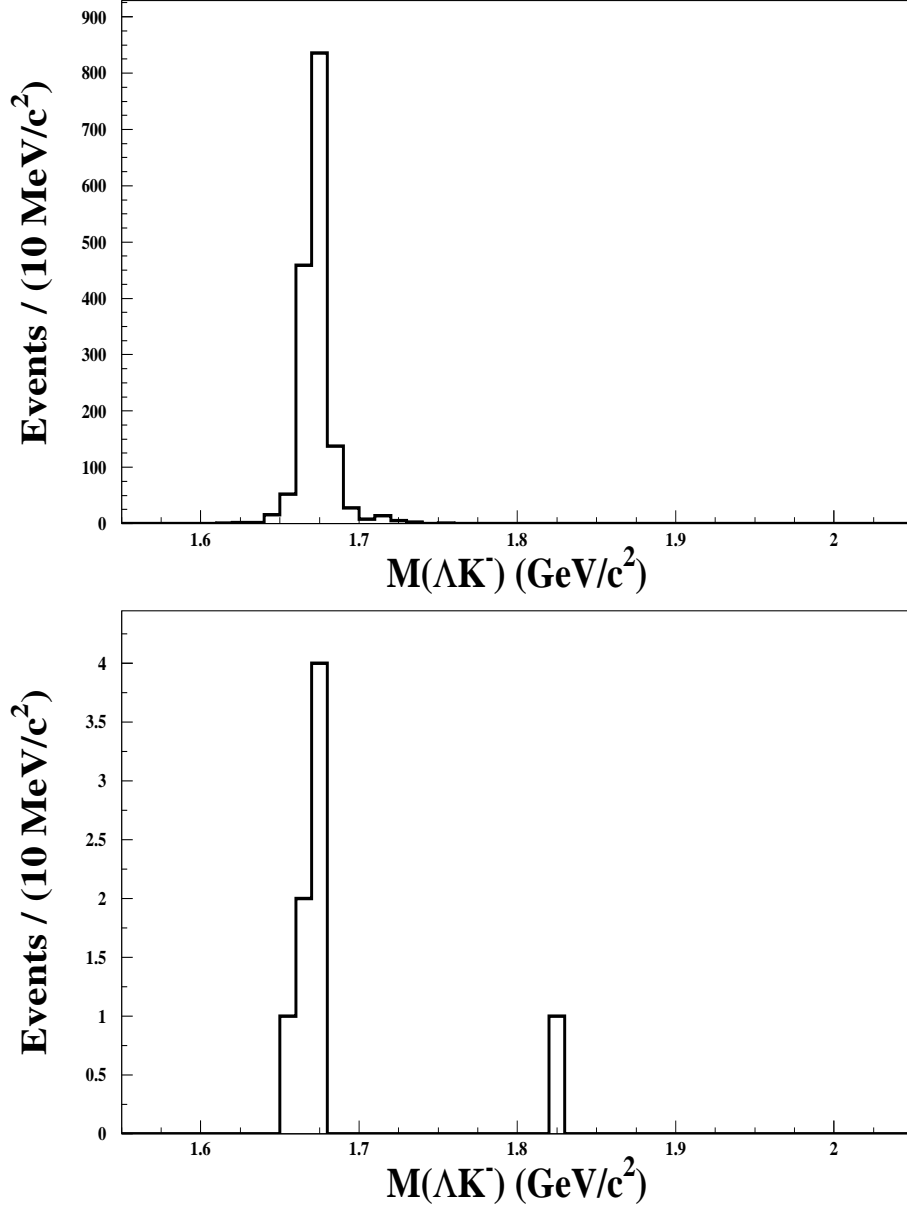


Figure 5.10: ΛK^- invariant mass spectra: (a) from signal MC and (b) from data, under the constraints: $|M_{p\pi^-} - M_\Lambda| < 0.012 \text{ GeV}/c^2$, $|M_{\bar{p}\pi^+} - M_{\bar{\Lambda}}| < 0.012 \text{ GeV}/c^2$, $|M_{\bar{\Lambda}K^+} - M_{\bar{\Omega}^+}| < 0.025 \text{ GeV}/c^2$ and $(\chi_{4C}^2 < 20 \text{ or } \chi_{1C}^2 < 10)$ [83].

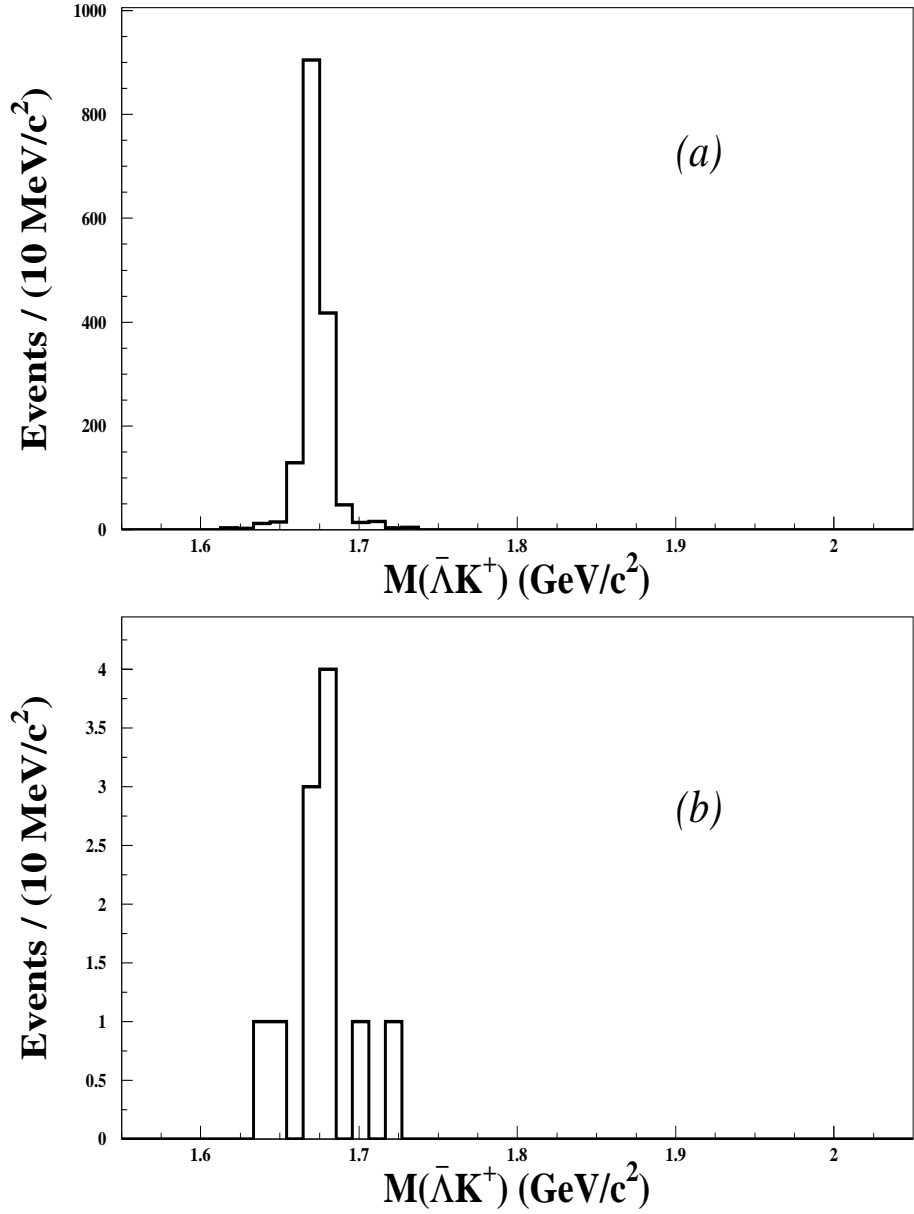


Figure 5.11: $\bar{\Lambda}K^+$ invariant mass distributions: (a) from signal MC and (b) from data, under the constraints: $|M_{p\pi^-} - M_{\Lambda}| < 0.012 \text{ GeV}/c^2$, $|M_{\bar{p}\pi^+} - M_{\bar{\Lambda}}| < 0.012 \text{ GeV}/c^2$, $|M_{\Lambda K^-} - M_{\Omega^-}| < 0.025 \text{ GeV}/c^2$ and ($\chi_{4C}^2 < 20$ or $\chi_{1C}^2 < 10$) [83].

The scatter plot of ΛK^- versus $\bar{\Lambda} K^+$ is shown in figure 5.12, under the constraints: $|M_{p\pi^-} - M_\Lambda| < 0.012$, $|M_{\bar{p}\pi^+} - M_{\bar{\Lambda}}| < 0.012$ and $\chi_{4C}^2 < 20$ or $\chi_{1C}^2 < 10$. A cluster of events can be clearly seen in the central mass region of Ω^- and $\bar{\Omega}^+$ (Fig. 5.12).

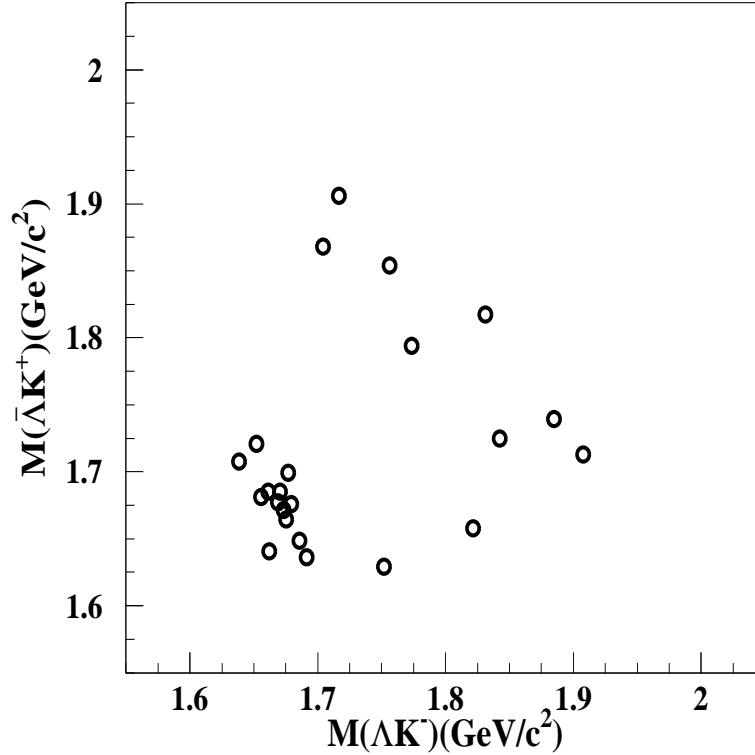


Figure 5.12: Scatter Plot of $\bar{\Lambda} K^+$ versus ΛK^- for data events, under the constraints: $|M_{p\pi^-} - M_\Lambda| < 0.012$ GeV/c², $|M_{\bar{p}\pi^+} - M_{\bar{\Lambda}}| < 0.012$ GeV/c² and $\chi_{4C}^2 < 20$ (for those events which are obtained through 4C kinematic fit) or $\chi_{1C}^2 < 10$ (for events obtained via 1C kinematic fit) [83].

5.9 Background Analysis

After final selection of ΛK^- and $\bar{\Lambda} K^+$ invariant mass distributions, several $\psi(2S)$ decay channels were investigated to examine background in the signal and sideband regions. For this purpose, we used 14×10^6 $\psi(2S)$ inclusive MC as well as exclusive

MC samples. From the inclusive MC sample, negligible background was found in the signal region. The sideband regions are slightly affected by the decay process $\psi(2S) \rightarrow \Lambda\bar{\Lambda}\phi(1020)$ with $\phi(1020) \rightarrow K^+K^-$. In exclusive background analysis, we used some $\psi(2S)$ decay channels: $\psi(2S) \rightarrow \Lambda\bar{\Lambda}\pi^+\pi^-$, $\psi(2S) \rightarrow \Lambda\bar{\Lambda}\phi(1020)$, $\phi \rightarrow K^+K^-$, $\psi(2S) \rightarrow \Xi^-\bar{\Xi}^+, \Xi^- \rightarrow \Lambda\pi^-, \bar{\Xi}^+ \rightarrow \bar{\Lambda}\pi^+$ and $\psi(2S) \rightarrow \Lambda\bar{p}K^+\pi^+\pi^-$. In each case, MC sample of 10000 events was obtained by using HOWL generator. Background events normalized to 14 million $\psi(2S)$ data, were found to be negligible, as shown in Table 5.1.

Table 5.1: The background estimates for $\psi(2S) \rightarrow \Omega^-\bar{\Omega}^+, \Omega^- \rightarrow \Lambda K^-, \bar{\Omega}^+ \rightarrow \bar{\Lambda} K^+$ [83]

Channels	N_{gen}	Br ($\times 10^{-4}$)	N_{obs}	(Normalized to 14 M)
$\psi(2S) \rightarrow \Lambda\bar{\Lambda}\pi^+\pi^-$	10000	2.8 ± 0.6	0	0
$\psi(2S) \rightarrow \Lambda\bar{\Lambda}\phi(1020)$	10000	—	8	—
$\psi(2S) \rightarrow \Lambda\bar{p}K^+\pi^+\pi^-$	10000	1.8 ± 0.4	0	0
$\psi(2S) \rightarrow \Xi^-\bar{\Xi}^+$	10000	1.5 ± 0.7	0	0

5.10 Statistical Significance of Ω^- and $\bar{\Omega}^+$ Signals

After background analysis, we determined statistical significant levels of Ω^- and $\bar{\Omega}^+$. As negligible background was found, phase space background from $\psi(2S) \rightarrow$

$\Lambda\bar{\Lambda}K^+K^-$ was taken as background shape in making fits to ΛK^- and $\bar{\Lambda}K^+$ invariant mass spectra. In order to determine the significance levels, we made two types of maximum likelihood fits to each of the ΛK^- and $\bar{\Lambda}K^+$ invariant mass distributions (Fig. 5.13 to Fig. 5.16). First fit was made by using respective fixed Monte Carlo histogram as signal shape and phase space background shape obtained from 0.25 million MC sample of $\psi(2S) \rightarrow \Lambda\bar{\Lambda}K^+K^-$. The second fit was made using phase space background shape only, assuming no signal. In order to obtain the significance levels, the values of log likelihood from the two fit types, were used in the following relation [88]:

$$S = \sqrt{|2\ln[\mathcal{L}_{max}(s+b)] - 2\ln[\mathcal{L}_{max}(b)]|}, \quad (5.1)$$

where $-2\ln[\mathcal{L}_{max}(s+b)]$ represents the value of maximum log likelihood when both the signal as well as background are used in the fit and $-2\ln[\mathcal{L}_{max}(b)]$ represents the maximum log likelihood value when no signal is used. The statistical significance levels of Ω^- and $\bar{\Omega}^+$ signals were determined to be 5.3σ and 4.6σ , respectively.

5.11 Detection Efficiency

The MC invariant mass distributions of ΛK^- and $\bar{\Lambda}K^+$ were used to determine detection efficiencies of Ω^- and $\bar{\Omega}^+$ signals. Under final selection criteria the detection (reconstruction) efficiency of Ω^- was determined to be 8.3%.

Detail about the detection efficiency of Ω^- is given as:

The number of Ω^- events obtained under final selection criteria were used in the

following relation:

$$\epsilon_{MC} = \frac{N_{sel}^{MC}}{N_{gen}^{MC}} \times 100,$$

where ϵ_{MC} represents the MC detection efficiency, N_{sel}^{MC} is for number of selected MC events after final selection and N_{gen}^{MC} denotes total number of exclusive MC events of the signal channel. The value of N_{gen}^{MC} is calculated as below:

$$N_{gen}^{MC} = [Br(\Omega^- \rightarrow \Lambda K^-)]^2 \times [Br(\Lambda \rightarrow p\pi^-)]^2 \times N_{incl}^{MC} \quad (5.2)$$

where $N_{incl}^{MC} = 10^5$, $Br(\Omega^- \rightarrow \Lambda K^-) = (67.8 \pm 0.7)\%$ [31], $Br(\Lambda \rightarrow p\pi^-) = (63.9 \pm 0.5)\%$ [31], $N_{sel}^{MC} = 1564$ (for $\alpha = 0$) under final selection criteria. The value of N_{gen}^{MC} is determined to be 18769.8. Thus the detection efficiency is calculated to be 8.3%.

5.12 Determination of Branching Fraction

The value of $Br(\psi(2S) \rightarrow \Omega^- \bar{\Omega}^+)$ was determined using the following steps:

- A likelihood fit was made to the invariant mass distribution of ΛK^- , taking fixed MC histogram as signal shape and phase space invariant mass distribution of ΛK^- as background shape (Fig. 5.13). The fit result gave ratio of number of signal events in data sample to the selected number of signal events in MC i.e.,

$$\frac{N_{obs}^{Data}}{N_{sel}^{MC}} = (4.50 \pm 1.75) \times 10^{-3}.$$

- The branching fraction was calculated considering the following relation [74]:

$$Br(\psi(2S) \rightarrow \Omega^- \bar{\Omega}^+) = \frac{N_{obs}^{Data}}{\epsilon_{MC} [Br(\Omega^- \rightarrow \Lambda K^-)]^2 \times [Br(\Lambda \rightarrow p\pi^-)]^2 N_{\psi(2S)}^{Data}}. \quad (5.3)$$

Substituting the value of ϵ_{MC} , relation 5.3 can be written as:

$$Br(\psi(2S) \rightarrow \Omega^- \bar{\Omega}^+) = \frac{N_{obs}^{Data}}{\frac{N_{sel}^{MC}}{N_{gen}^{MC}} [Br(\Omega^- \rightarrow \Lambda K^-)]^2 \times [Br(\Lambda \rightarrow p\pi^-)]^2 N_{\psi(2S)}^{Data}} \quad (5.4)$$

Now relation 5.4 can be arranged as:

$$Br(\psi(2S) \rightarrow \Omega^- \bar{\Omega}^+) = \frac{\frac{N_{obs}^{Data}}{N_{sel}^{MC}} N_{gen}^{MC}}{[Br(\Omega^- \rightarrow \Lambda K^-)]^2 \times [Br(\Lambda \rightarrow p\pi^-)]^2 N_{\psi(2S)}^{Data}} \quad (5.5)$$

As

$$\frac{N_{gen}^{MC}}{[Br(\Omega^- \rightarrow \Lambda K^-)]^2 \times [Br(\Lambda \rightarrow p\pi^-)]^2} = N_{incl}^{MC},$$

the relation 5.5 becomes:

$$Br(\psi(2S) \rightarrow \Omega^- \bar{\Omega}^+) = \frac{\frac{N_{obs}^{Data}}{N_{sel}^{MC}} N_{incl}^{MC}}{N_{\psi(2S)}^{Data}} \quad (5.6)$$

Substituting the values of $\frac{N_{obs}^{Data}}{N_{sel}^{MC}}$, N_{incl}^{MC} and $N_{\psi(2S)}^{Data}$ in relation 5.6, we obtain

$$Br(\psi(2S) \rightarrow \Omega^- \bar{\Omega}^+) = \frac{(4.50 \pm 1.75) \times 10^{-3} \times 10^5}{14 \times 10^6} = (3.21 \pm 1.25) \times 10^{-5},$$

where the error is statistical.

MINUIT Likelihood Fit to Plot 7&0

File: omom.his 24-MAY-2009 20:22
 Plot Area Total/Fit 8.0000 / 8.0000 Fit Status 3
 Func Area Total/Fit 8.0005 / 8.0005 E.D.M. 1.282E-07

Likelihood = 9.5
 $\chi^2 = 29.0$ for 50 - 2 d.o.f., C.L. = 98.7%

Errors	Function	Normal errors	Parabolic	Minos	
	Function 1: Histogram	5.0			
NORM		$4.50833E-03$	$\pm 1.7513E-03$	- 0.000	+ 0.000
	Function 2: Histogram	6.0	No errors		
NORM		$3.55196E-04$	$\pm 3.5351E-04$	- 0.000	+ 0.000

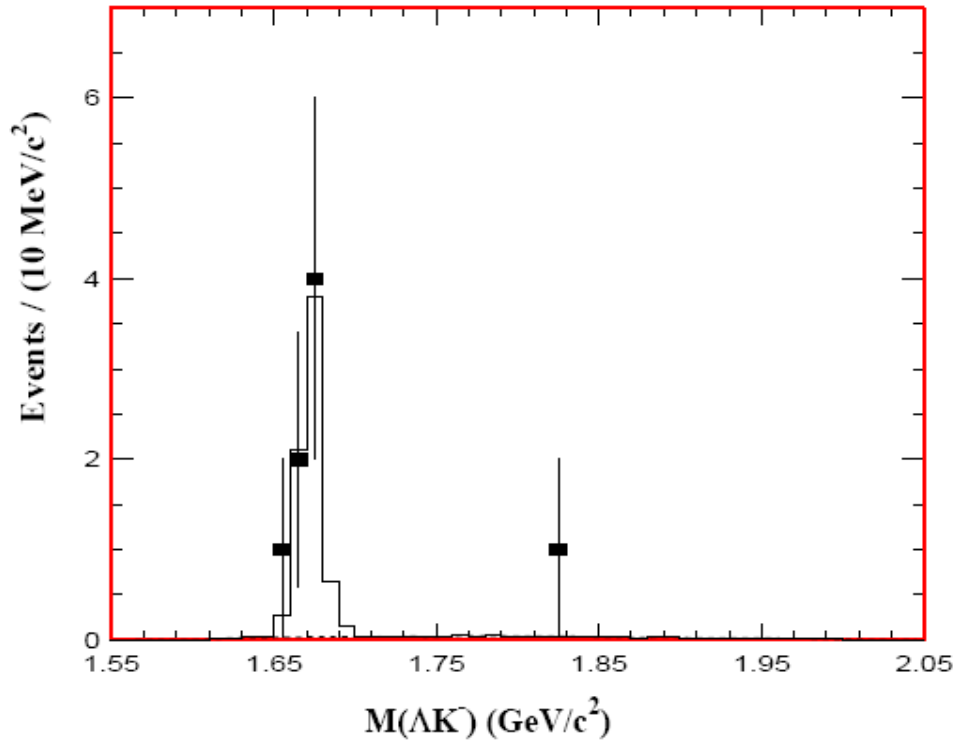


Figure 5.13: Fit to ΛK^- invariant mass spectrum, using signal MC histogram of ΛK^- invariant mass spectrum as signal shape and histogram of $\Lambda \bar{\Lambda} K^+ K^-$ invariant mass spectrum from $\psi(2S) \rightarrow \Lambda \bar{\Lambda} K^+ K^-$ as phase space background shape. The squares with error bars represent data. Background in the signal region is negligible as shown in the figure ([82], [83]).

MINUIT Likelihood Fit to Plot

7&0

File: omom.his

24-MAY-2009 20:23

Plot Area Total/Fit 8.0000 / 8.0000

Fit Status 3

Func Area Total/Fit 7.9998 / 7.9998

E.D.M. 5.815E-09

Likelihood = 37.1

$\chi^2 = 82.9$ for 50 - 1 d.o.f.,

C.L.=0.176 %

Errors Parabolic

Minos

Function 1: Histogram 6 0 No errors

NORM 2.40308E-03 \pm 8.4962E-04

- 0.000

+ 0.000

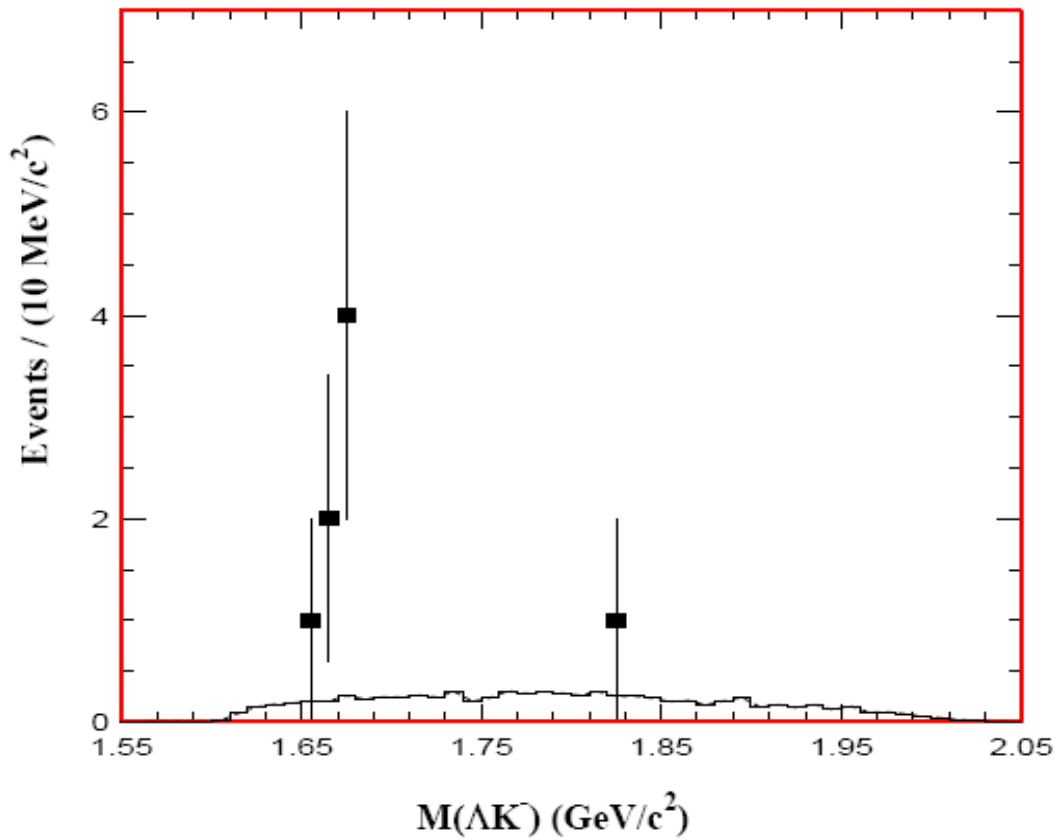


Figure 5.14: Fit to ΛK^- invariant mass spectrum using only histogram of ΛK^- invariant mass spectrum from $\psi(2S) \rightarrow \Lambda \bar{\Lambda} K^+ K^-$ as phase space background shape (assuming no signal). The squares with error bars represent data ([82], [83]).

MINUIT Likelihood Fit to Plot

7&0

File: omom.his
 Plot Area Total/Fit 11.000 / 11.000
 Func Area Total/Fit 11.000 / 11.000
 Likelihood = 19.5
 $\chi^2 = 31.2$ for 48 - 2 d.o.f., C.L. = 95.4%
 Errors Parabolic Minos
 Function 1: Histogram 5 0 Normal errors
 NORM 4.64166E-03 \pm 1.8425E-03 - 0.000 + 0.000
 Function 2: Histogram 6 0 No errors
 NORM 1.21684E-03 \pm 6.6683E-04 - 0.000 + 0.000

24-MAY-2009 20:58
 Fit Status 3
 E.D.M. 2.525E-08

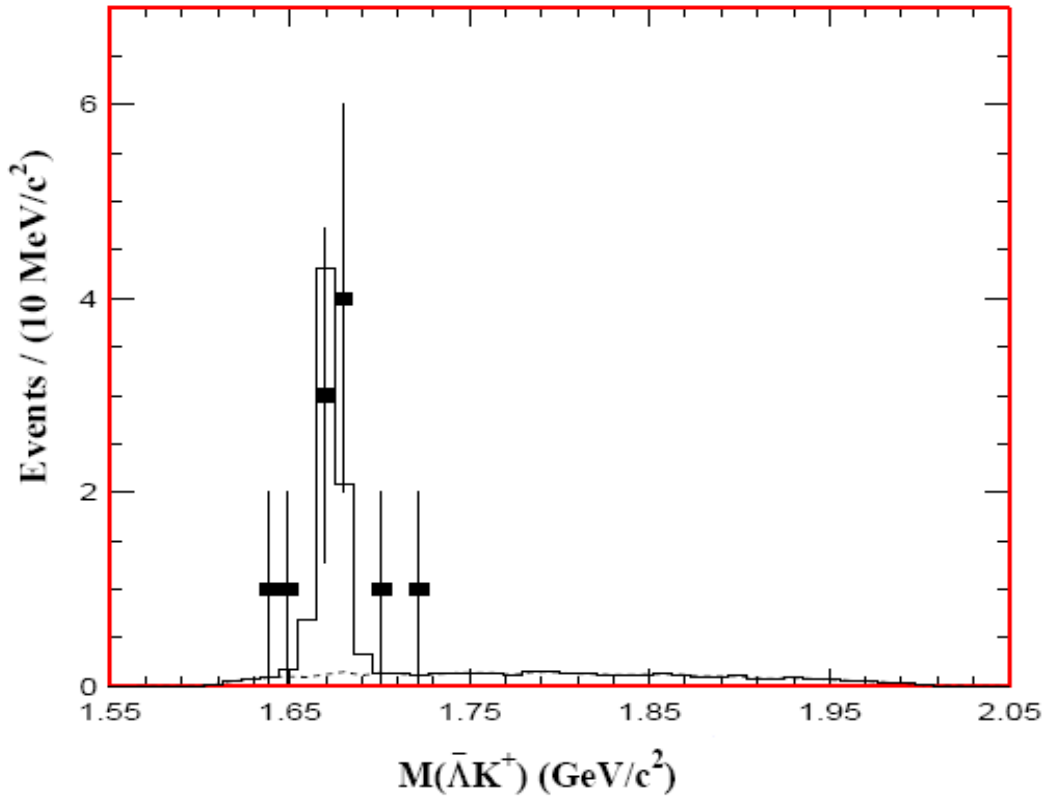


Figure 5.15: Fit to $\bar{\Lambda}K^+$ invariant mass spectrum, using signal MC histogram of $\bar{\Lambda}K^+$ invariant mass spectrum as signal shape and histogram of $\bar{\Lambda}K^+$ invariant mass spectrum from $\psi(2S) \rightarrow \Lambda\bar{\Lambda}K^+K^-$ as phase space background shape. The squares with error bars represent data. Background in the signal region is not so large as shown in the figure ([82], [83]).

MINUIT Likelihood Fit to Plot

7&0

File: omom.his
 Plot Area Total/Fit 11.000 / 11.000
 Func Area Total/Fit 11.000 / 11.000

24-MAY-2009 20:57
 Fit Status 3
 E.D.M. 3.805E-10

Likelihood = 40.7

$\chi^2 = 67.7$ for 48 - 1 d.o.f.,

C.L. = 2.6%

Errors Parabolic Minos

Function 1: Histogram 6 0 No errors

NORM 3.37318E-03 \pm 1.0171E-03 - 0.000 + 0.000

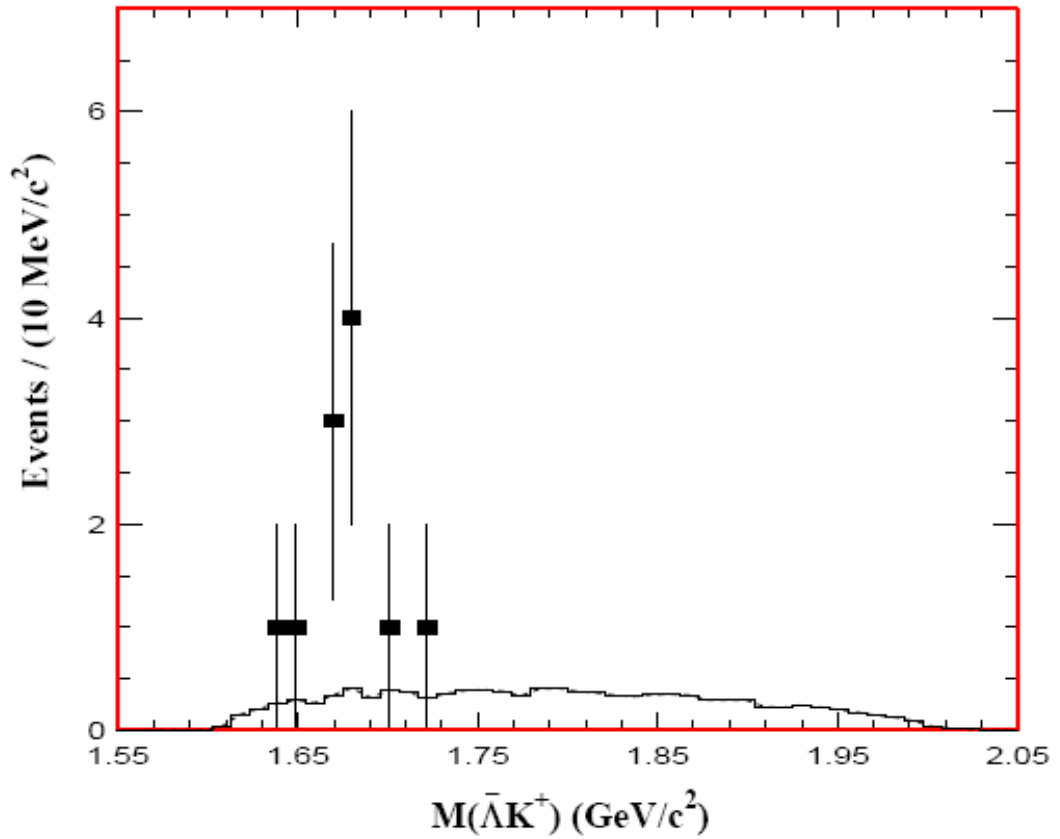


Figure 5.16: Fit to $\bar{\Lambda}K^+$ invariant mass spectrum using only histogram of $\bar{\Lambda}K^+$ invariant mass spectrum from $\psi(2S) \rightarrow \Lambda\bar{\Lambda}K^+K^-$ as phase space background shape (assuming no signal). The squares with error bars represent data ([82], [83]).

The overall detection efficiency for the signal channel $\psi(2S) \rightarrow \Omega^-\bar{\Omega}^+$, under mass and χ^2 constraints, obtained from 4C or 1C fit is 8.3%. The detection efficiency from 4C fit is 1.7% and that from 1C fit is 6.6%. We use either 4C or 1C fit for an event with six or five identified particles, therefore contributions to the total systematic error from 4C and 1C fits will be according to their proportion of detection efficiency. There will be two total systematic errors; one when 4C fit is used and the other when 1C fit is employed. These total systematic errors are determined separately and then added directly to get total systematic error in branching fraction. The total systematic error for 4C fit result is estimated to be 36% through quadrature rule (Table 5.2), while the total systematic error for 1C fit results is estimated to be 28.5% (Table 5.2) [89].

In order to determine total systematic error in the branching fraction, we first calculate the total systematic errors for 4C and 1C fit results, separately, into the branching fraction. The systematic error for 4C fit result and 1C fit result, is calculated by considering $Br(\psi(2S) \rightarrow \Omega^-\bar{\Omega}^+) = (3.21 \pm 1.25) \times 10^{-5}$:

Total systematic error in the value of branching fraction, for 4C fit results

$$= 3.21 \times \frac{1.7}{8.3} \times 0.36 \times 10^{-5} = 0.24 \times 10^{-5}$$

Total systematic error in the value of branching fraction, for 1C fit results

$$= 3.21 \times \frac{6.6}{8.3} \times 0.285 \times 10^{-5} = 0.73 \times 10^{-5}$$

Now the total systematic error can be estimated by directly adding them i.e., $0.24 + 0.73 = 0.97$. Therefore $Br(\psi(2S) \rightarrow \Omega^-\bar{\Omega}^+) = (3.21 \pm 1.25(stat) \pm 0.97(sys)) \times 10^{-5}$.

5.13 Systematic Error Analysis

The candidate events for the signal channel have been selected in two ways; events with six charge tracks or events with five charge tracks (one charge track missing). For events with six charge tracks, we perform 4C kinematic fit, whereas for events with five charge tracks we perform 1C kinematic fit. Therefore the systematic error analysis for 4C kinematic fit results and 1C kinematic fit results is made separately. In the systematic error analysis, the following sources of uncertainties are considered.

- Models of hadron interaction
- Track identification
- MDC tracking
- 4C kinematic fit
- 1C kinematic fit
- Angular distribution of events
- Monte Carlo statistics
- Intermediate branching fractions
- Total number of $\psi(2S)$ data events

These sources of uncertainty are described in the following subsections:

5.13.1 Models of Hadron Interaction

The systematic error was obtained by using MC statistics obtained from two hadron interaction models; GCALOR [90] and FLUKA [91]. The value of detection efficiency varies with the type of these models of hadron interaction. In order to estimate the systematic error due to hadron interaction models, we generated 4 pairs of MC samples for $\alpha = 0$, $\alpha = 0.5$, $\alpha = 1.0$ and $\alpha = -1.0$. Each pair of MC sample was obtained by using GCALOR and FLUKA hadron interaction models for each value of α . For each value of α , the systematic error between GCALOR and FLUKA MC samples was estimated, thus getting four values for the systematic error for 4C and 1C kinematic fit results separately:

For 4C kinematic fit results these errors are; 8.4% for $\alpha = 0$, 11.3% for $\alpha = 0.5$, 9.2% for $\alpha = 1.0$ and 22.6% for $\alpha = -1.0$. The largest of these four values i.e., 22.6% was taken as systematic error for 4C kinematic fit results.

For 1C kinematic fit results these errors are; 7.2% for $\alpha = 0$, 9.9% for $\alpha = 0.5$, 15.4% for $\alpha = 1.0$ and 11.9% for $\alpha = -1.0$. The largest of these four values i.e., 15.4% was taken as systematic error for 1C kinematic fit results.

5.13.2 Particle Identification

The systematic uncertainty arising from particle identification of charge tracks for p , \bar{p} , π^- , π^+ , K^+ and K^- , was taken as 6% for 4C kinematic fit results and 5% for 1C kinematic fit results, at the rate of 1% per charged track, from earlier systematic error analysis results [47].

5.13.3 MDC Tracking

There are six charged particles in the final state of $\psi(2S) \rightarrow \Omega^-\bar{\Omega}^+, \Omega^- \rightarrow \Lambda K^-, \bar{\Omega}^+ \rightarrow \bar{\Lambda} K^+$, namely; $p, \bar{p}, \pi^+, \pi^-, K^+$ and K^- . The selection of candidate events involves events with six charge tracks or events with 5 charge tracks. Therefore, according to the detailed study of error analysis, already performed, a systematic error of 2% per charged track was adopted as MDC tracking error [47]. Thus an error of 12% for 4C kinematic fit results, and 10% for 1C kinematic fit results was used as systematic error due to MDC tracking.

5.13.4 4C Kinematic Fit

The systematic error from 4C kinematic fit was studied through analysis of $J/\psi \rightarrow \Xi^-\bar{\Xi}^+$ ($\Xi^- \rightarrow \Lambda\pi^-, \bar{\Xi}^+ \rightarrow \bar{\Lambda}\pi^+, \Lambda \rightarrow p\pi^-$ and $\bar{\Lambda} \rightarrow \bar{p}\pi^+$) decay channel. The systematic error in this case (for 6 charge track system) was estimated to be 19.1% by comparing relative efficiencies of MC and data results, obtained with and without 4C fit.

5.13.5 1C Kinematic Fit

Systematic error due to 1C fit was estimated by comparing the MC and DATA relative efficiencies of results without kinematic fit (no 4C kinematic fit) and 1C kinematic fit results obtained from the analysis of $J/\psi \rightarrow \Xi^-\bar{\Xi}^+$ ($\Xi^- \rightarrow \Lambda\pi^-, \bar{\Xi}^+ \rightarrow \bar{\Lambda}\pi^+, \Lambda \rightarrow p\pi^-$ and $\bar{\Lambda} \rightarrow \bar{p}\pi^+$). The error was estimated to be 14.6%.

5.13.6 Angular Distribution of Events

In order to estimate this systematic error, we obtained four MC samples by using GCALOR model for four values of α i.e 0.0 (uniform distribution), 0.5, 1.0 and -1.0. The statistics in ΛK^- invariant mass distribution for $\alpha = 0.0$ after final selection criteria was compared with those for $\alpha = 0.5$, $\alpha = 1.0$ and $\alpha = -1.0$, thus getting three values for the systematic error due to angular distribution for 4C kinematic fit results and 1C kinematic fit results separately:

For 4C kinematic fit results, these error values are; 14.4% for $\alpha = 0$ and $\alpha = -1.0$, 0% for $\alpha = 0$ and $\alpha = 0.5$ and 8.7% for $\alpha = 0$ and $\alpha = +1.0$. Thus giving maximum error value of 14.4%.

For 1C kinematic fit results, these error values are; 14.7% for $\alpha = 0$ and $\alpha = -1$, 4.3% for $\alpha = 0$ and $\alpha = 0.5$ and 3.4% for $\alpha = 0$ and $\alpha = +1.0$. Thus giving maximum error value of 14.7%.

5.13.7 Monte Carlo Statistics

For estimating uncertainty from this source, we generated 250,000 inclusive MC events by using P2BB generator. It gave 46,975 MC generated events for the signal channel; $\psi(2S) \rightarrow \Omega^- \bar{\Omega}^+, \Omega^- \rightarrow \Lambda K^-, \bar{\Omega}^+ \rightarrow \bar{\Lambda} K^+, \Lambda \rightarrow p\pi^-, \bar{\Lambda} \rightarrow \bar{p}\pi^+$. The monte carlo statistical error was estimated by using the detection efficiency (from MC results of GCALOR with $\alpha = 0.0$) and the total number of events of $\psi(2S) \rightarrow \Omega^- \bar{\Omega}^+, \Omega^- \rightarrow \Lambda K^-, \bar{\Omega}^+ \rightarrow \bar{\Lambda} K^-, \Lambda \rightarrow p\pi^-$ and $\bar{\Lambda} \rightarrow \bar{p}\pi^+$ generated by using P2BB generator, in

the following relation:

MC statistical error

$$= \frac{\Delta\epsilon}{\epsilon} = \frac{\sqrt{\frac{\epsilon(1-\epsilon)}{N_{gen}^{MC}}}}{\epsilon},$$

where ϵ and N_{gen}^{MC} represent the detection efficiency and total number of signal MC generated events. The overall detection efficiency (from 4C as well as 1C kinematic fit results) is 8.7%.

For 4C kinematic fit results, the detection efficiency is 1.7%, thus giving MC statistical uncertainty of 3.5%.

For 1C kinematic fit results, the detection efficiency is 7%, therefore giving 1.7% as MC statistical error.

5.13.8 Intermediate Branching Fractions

The systematic uncertainty arising from the branching fractions of intermediate resonances was obtained from the uncertainties in these branching fractions, according to their PDG values [31]:

$$Br(\Omega^- \rightarrow \Lambda K^-) = (67.8 \pm 0.7)\%$$

$$Br(\Lambda \rightarrow p\pi^-) = (63.9 \pm 0.5)\%$$

Because $\bar{\Omega}^+ \rightarrow \bar{\Lambda} K^+$ and $\bar{\Lambda} \rightarrow \bar{p}\pi^+$ are also involved, the uncertainties from $[Br(\Omega^- \rightarrow \Lambda K^-)]^2$ and $[Br(\Lambda \rightarrow p\pi^-)]^2$ are calculated as 2.1% and 1.5% respectively. Their combined effect is evaluated through quadrature rule [89] to be 2.4% (same for 4C kinematic fit results as well as 1C kinematic fit results).

5.13.9 Total Number of $\psi(2S)$ Data Events

While calculating branching fraction of $\psi(2S) \rightarrow \Omega^-\bar{\Omega}^+$, we used 14×10^6 as total number of $\psi(2S)$ data events. The total number of $\psi(2S)$ has been estimated to be $(14 \pm 0.6) \times 10^6$ by using inclusive events of hadrons with an uncertainty of 4.3% [74] (for each of 4C kinematic fit results and 1C kinematic fit results).

Systematic uncertainties obtained for 4C kinematic fit results and 1C kinematic fit results are listed in Table 5.2. For 4C kinematic fit results, the total uncertainty from quadrature rule [89] comes to be 36% and for 1C kinematic fit results, the total uncertainty through quadrature rule is 28.5%.

Table 5.2: Systematic uncertainties (%) in the branching fraction ([82], [83])

Source of Uncertainty	4C Fit Uncertainty	1C Fit Uncertainty
Models of Hadron Interaction	22.6	15.4
Particle Identification	6	5
MDC tracking	12	10
Kinematic Fit	19.1	14.6
Angular Distribution	14.4	14.7
MC Statistics	3.5	1.7
Intermediate Resonances	2.4	2.4
Total Number of $\psi(2S)$ events	4.3	4.3
	Total = 36	Total = 28.5

Chapter 6

DISCUSSION AND CONCLUSIONS

Current work is of prime importance both from theoretical and experimental point of view. This study will help us in strengthening our belief in QCD and quark model.

Some of the immediate implications of the evidence of this decay process are:

1. Quark model has always played an important role in the understanding of 'strong physics'. It is interesting to note that during the past four decades, many experimental observations in particle physics were consistent with the quark model. At its earliest stage, quark model predicted some hadrons along with their properties which were only possible through violation of famous 'Pauli exclusion principle'. These hadrons were discovered experimentally with properties as predicted by the quark model, leaving a clue about something new:

either Pauli's exclusion principle was wrong or some physics was hidden behind the existence of such hadrons like Ω^- . From the experimental verification of such hadrons, it was imperative to think about some new property of their constituents called quarks, while maintaining our faith in Pauli's exclusion principle. Consequently the 'color quantum number' of quarks was introduced to justify the existence of the anomalous hadron species including Ω^- . The evidence or observation of Ω^- in any decay process is therefore of prime importance in our belief in color quantum number and thus QCD.

2. Evidence of the current decay process strengthens the position of strange hadrons in the quark model. It is because, Ω^- accompanied with $\bar{\Omega}^+$ is prominently produced through strong decay of $\psi(2S)$ and can decay only through weak interaction. Thus, with large statistics, the weak interaction can be better studied through this process.
3. As Ω^- is produced mainly through strong interaction and decays through only weak interaction, it may leave a hint about the relationship of weak force with the strong force. As weak and electromagnetic forces are already unified, therefore, a clue about the unification of three forces may be found through study of the current decay process using huge statistics of data.

In view of the importance of this decay mode, an in-depth analysis with high precision is necessary. As a start in this direction, several measures were taken. As mentioned earlier, in order to determine the possibility of observation of $\psi(2S) \rightarrow \Omega^- \bar{\Omega}^+$ decay process by BESII detector, we have used the dominant decay modes of Ω^- ($\bar{\Omega}^+$):

$\Omega^- \rightarrow \Lambda K^-$ ($\bar{\Omega}^+ \rightarrow \bar{\Lambda} K^+$) and of Λ ($\bar{\Lambda}$): $\Lambda \rightarrow p\pi^-$ ($\bar{\Lambda} \rightarrow \bar{p}\pi^+$). The final state of $\psi(2S) \rightarrow \Omega^-\bar{\Omega}^+$ has six charged particles: proton (p), pion (π^-), kaon (K^-), antiproton (\bar{p}), pion (π^+) and kaon (K^+).

In the first step, candidate events were obtained through Monte Carlo detector simulation of the signal process. As the purpose of a detector simulation of certain process is to mimic 'real events', the simulation results should approximate well the 'real decay process'. In this pursuit, detection efficiency of $\psi(2S) \rightarrow \Omega^-\bar{\Omega}^+$ was improved to minimize the chances of loss of events. It was achieved by placing a special focus on low momentum particles which are prone to be 'missed out'. Some of the low momentum particles may not be recorded by the detector due to insufficient measured information. Due to such a loss in measurement by MDC or TOF system of the detector, some of the actual events may be skipped. Thus, for low momentum particles, the chances of loss of events is increased. In order to minimize the loss of 'actual events', some important steps were taken. An important and very significant step was to consider candidate events with missing particles from the final state. We have considered the case of events having *one* missing particle in the final state. As a result of this selection, the detection efficiency increased from 1.7% (for events having all six charge tracks in the final state) to 8.3% (for events having either six or five charge tracks in the final state). The increased detection efficiency enhances the chances of background events. However, due to resonances of very small decay widths i.e., Ω^- , $\bar{\Omega}^+$, Λ and $\bar{\Lambda}$, when mass and χ^2 constraints are applied to get invariant mass distributions of ΛK^- (for Ω^-) and $\bar{\Lambda} K^+$ (for $\bar{\Omega}^+$), the chances of background events

were reduced.

For greater detection efficiency, in addition to consideration of events with one missing track, the particles in the final state were identified by using only their dE/dx information. When both the dE/dx information and TOF information is used in particle identification, the detection efficiency was found to decrease. It is because the particles having low momentum may lack TOF information, increasing the chances of incorrect assignment of particle hypothesis to a charge track.

6.1 CONCLUSIONS

In the light of our analysis results and above mentioned discussion, the following conclusions are drawn:

1. Using 14 million $\psi(2S)$ decays recorded by BESII detector at BEPC, the branching fraction of $\psi(2S) \rightarrow \Omega^- \bar{\Omega}^+$ decay process, is determined to be $(3.21 \pm 1.25(stat) \pm 0.97(sys)) \times 10^{-5}$. The statistical significance levels of Ω^- and $\bar{\Omega}^+$ signals, were determined to be 5.3σ and 4.6σ , respectively.
2. Our result of $Br(\psi(2S) \rightarrow \Omega^- \bar{\Omega}^+)$ is consistent with the upper limits reported by BES and CLEO Collaborations at 90% confidence level: 7.3×10^{-5} and 1.6×10^{-4} , respectively. This consistency expresses that technique of selecting events with one missing track also, has been very successful.
3. Precise measurements of high energy processes demand large amount of data.

This can be achieved/enhanced through improved experimental setup with better detector resolutions. Alternately, this task can be achieved by increasing detection efficiency with minimum possibility of background events. In our study the technique of selecting events with one missing particle also, was employed. This resulted in four-fold increase in detection efficiency.

4. The systematic error in the branching fraction will be reduced by using large data statistics at BESIII and better analysis tools: MC generators, GEANT4 detector simulation toolkit and reconstruction software etc.
5. BESIII experiment will provide huge statistics of $\psi(2S)$ decays in the near future. About 200 million $\psi(2S)$ events have already been recorded. This number is expected to further increase by about an order of magnitude. The data will thus help us perform more precise measurement of $Br(\psi(2S) \rightarrow \Omega^-\bar{\Omega}^+)$, with low statistical error.

Bibliography

- [1] M. B. Robinson, T. Ali and G. B. Cleaver, *A Simple Introduction to Particle Physics Part II - Geometric Foundations and Relativity*, arXiv:0908.1395v1 [hep-th].
- [2] M. B. Robinson et al., *A Simple Introduction to Particle Physics*, arXiv:0810.3328v1 [hep-th].
- [3] I. Gonzalez and M. Loewe, *Feynman Diagrams and a Combination of the Integration by Parts (IBP) and the Integration by Fractional Expansion (IBFE) Techniques*, arXiv:0909.3493v2 [hep-th].
- [4] U. Reinosa and J. Serreau, *2PI functional techniques for gauge theories*, arXiv:0906.2881v1 [hep-ph].
- [5] R. J. Szabo, *Perturbation Theory and Techniques*, arXiv:hep-th/0505139v2.
- [6] H. Kroger et al., *Spectrum and Wave Functions of Excited States in Lattice Gauge Theory*, arXiv:0902.2944v1 [hep-lat].

- [7] B. Svetitsky, *Lattice gauge theory in technicolor*, arXiv:0901.2103v1 [hep-lat]., Talk given at PANIC 2008, 9-14 Nov 2008, Eilat, Israel.
- [8] F. Paradis et al., *Monte Carlo Hamiltonian of Lattice Gauge Theory*, Mod. Phys. Lett. A22, (2007) 565-572, arXiv:hep-lat/0508010v1.
- [9] M. Loan, X. Luo and Zhi-Huan Luo, *Monte Carlo study of glueball masses in the Hamiltonian limit of $SU(3)$ lattice gauge theory*, Int. J. Mod. Phys. A21, (2006) 2905-2936, arXiv:hep-lat/0503038v2.
- [10] F. Paradis et al., *Measure of the Path Integral in Lattice Gauge Theory*, Phys. Rev. D71, (2005) 077502, arXiv:hep-lat/0503028v1.
- [11] E. Sauvan, *Searches For New Physics with High Energy Colliders*, arXiv:0910.4509v1 [hep-ex].
- [12] T. Lari et al., *Collider aspects of flavour physics at high Q* , Eur. Phys. J. C57, (2008) 183-308.
- [13] J. List, *Physics at the International Linear Collider*, arXiv:hep-ex/0605087v1.
- [14] G. Chiarelli, *Searches for New Physics at Colliders*, AIP Conf. Proc. 815, (2006) 268-279, arXiv:hep-ex/0509037v1.
- [15] T. Han, *Collider Phenomenology: Basic Knowledge and Techniques*, arXiv:hep-ph/0508097v1.
- [16] B. Batell, M. Pospelov and A. Ritz, *Exploring Portals to a Hidden Sector Through Fixed Targets*, arXiv:0906.5614v2 [hep-ph].

- [17] J. D. Bjorken et al., *New Fixed-Target Experiments to Search for Dark Gauge Forces*, Phys. Rev. D80: 075018, 2009, arXiv:0906.0580v1 [hep-ph].
- [18] T. Adams et al., *Renaissance of the 1 TeV Fixed-Target Program*, arXiv:0905.3004v2 [hep-ex].
- [19] O.W. Greenberg, *The Color Charge Degree of Freedom in Particle Physics*, arXiv:0805.0289v2 [physics.hist-ph].
- [20] E. Minguzzi and C. Tejero Prieto, *A topological interpretation of the color charge*, Mod. Phys. Lett. A22, (2007) 1143-1152, arXiv:hep-th/0611167v2.
- [21] F. Becattini and R. Fries, *The QCD confinement transition: hadron formation*, arXiv:0907.1031v1 [nucl-th].
- [22] B. Layek, A. M. Srivastava and S. Sanyal, *Excited hadrons as a signal for quark-gluon plasma formation*, Int. J. Mod. Phys. A21, (2006) 3421, arXiv:hep-ph/0502109v2.
- [23] O. Actis et al., *Automated Reconstruction of Particle Cascades in High Energy Physics Experiments*, arXiv:0801.1302v2 [physics.data-an].
- [24] J.M. Butterworth, J.R. Ellis and A.R. Raklev, *Reconstructing Sparticle Mass Spectra using Hadronic Decays*, JHEP0705, (2007) 033, arXiv:hep-ph/0702150v1.
- [25] K. Kondo, *Dynamical Likelihood Method for Reconstruction of Quantum Process*, arXiv:hep-ex/0508035v2.

- [26] P. Zweber, for the BESIII Collaboration, *Charm Factories: Present and Future*, AIP Conf. Proc. 1182, (2009) 406-409, arXiv:0908.2157v1 [hep-ex].
- [27] (<http://www.ihep.ac.cn/english/E-Bepc/index.htm>)
- [28] S. F. Novaes, *Standard Model: An Introduction*, arXiv:hep-ph/0001283v1.
- [29] J. R. Letts, *A Measurement of Strange Baryon Production and Correlations in Hadronic Z^0 Decays*, PhD Thesis, University of California Riverside December 1993.
- [30] B. R. Martin and G. Shaw, *Particle Physics*, John Wiley & Sons Inc., second edition, 1997.
- [31] C. Amsler et al., *Review of Particle Physics*, Phys. Lett. B 667, (2008) 93-176. Particle Data Group.
- [32] D. H. Perkins, *Introduction to High Energy Physics*, Cambridge University Press, fourth Edition, 2000.
- [33] J. W. Rohlf, *Modern Physics from α to Z^0* , John Wiley & Sons Inc., first edition, 1994.
- [34] J. J. Aubert, et al., *Experimental Observation of a Heavy Particle J* , Phys. Rev. Lett. 33, (1974) 1404.
- [35] J. -E. Augustin, et al., *Discovery of a Narrow Resonance in e^+e^- Annihilation*, Phys. Rev. Lett. 33, (1974) 1406.

- [36] F. Halzen and A. D. Martin, *Quarks & Leptons: An Introductory Course in Modern Particle Physics*, John Willey & Sons Inc., first edition, 1984.
- [37] D. Kong, *Measurement of the Total cross section for hadronic production by ee annihilation at energies between 2-5 GeV/c²*, PhD Dissertation, University of Hawaii, Manoa, USA, 2000.
- [38] A. Lundborg, *The Charm of Excited Glue: Charmonium in e^+e^- and $p\bar{p}$ collisions*, PhD Dissertation, Acta Universitatis Upsaliensis, 2007.
- [39] J. Z. Bai et al., *The BES upgrade*, Nucl. Inst. and Meth., A458, (2001) 627637. BES Collaboration.
- [40] D. Haidt and P. Zerwas, *Review of Particle Physics*, Eur. Phys. J. C3, (1998) 244.
- [41] M. Ye and Z. Zheng, *BEPC, the Beijing Electron-Positron Collider*, Int. J. Mod. Phy. A 2, (1987) 1707.
- [42] X. Luo, *The 4th Annual BES Meeting*, BES Collaboration (IHEP, Beijing, 1995).
- [43] X. H. Mo et al., *Determination of $\psi(2S)$ total number by inclusive hadronic decay*, High Energy Phys. and Nucl. Phys. 27, (2004) 455. BES Collaboration.
- [44] S. P. Chi., High Energy Phys. and Nucl. Phys.28, (2004) 1135.
- [45] D. Pitman et al., *The Mark-III vertex chamber: Studies using DME*, Nucl. Instrum. Methods A 265, (1988) 85.

- [46] H. J. Bhabha, *The Scattering on Positrons by Electrons with Exchange on Diracs Theory of the Positron*, Proceedings of the Royal Society of London. Series A, Mathematical and Physical Sciences, Volume 154, Issue 881, (1936) 195-206.
- [47] M. Ablikim et al., *BESII detector simulation*, Nucl. Instrum. Methods A 552, (2005) 344. BES Collaboration.
- [48] N. Brambilla et al., *Heavy Quarkonium Physics*, CERN Yellow Report, CERN-2005-005, Geneva: CERN, 2005, arXiv:hep-ph/0412158v2.
- [49] W. M. Yao et al., *Review of Particle Physics*, Journ. Phys. G 33(1), 2006. Particle Data Group.
- [50] M.B. Voloshin, *Charmonium*, Prog. Part. Nucl. Phys. 61, (2008) 455-511.
- [51] R. E. Mitchell , *An Experimental Review of Charmonium*, arXiv:0810.3231v1 [hep-ex].
- [52] E. J. Eichten, K. Lane and C. Quigg, *B-Meson Gateways to Missing Charmonium Levels*, Phys. Rev. Lett. 89, (2002) 162002, arXiv:hep-ph/0206018.
- [53] S. -K. Choi, S. L. Olsen, et al, *Observation of a narrow charmonium-like state in exclusive $B^+ \rightarrow K^+\pi + \pi - J/\psi$ decays*, Phys. Rev. Lett. 91, (2003) 262001, arXiv:hep-ex/0309032. BELLE Collaboration.
- [54] P. YOCK, *The Gamma-Gamma Interaction: A Critical Test of the Standard Model*, Int. J. Mod. Phys. A24, (2009) 3276-3285.

- [55] F. A. Harris, *Light Hadron Spectroscopy and Charmonium*, 34th International Conference on High Energy Physics, Philadelphia, 2008, arXiv:0810.3045v1 [hep-ex].
- [56] B.G. Fulsom, *Recent Progress and Puzzles in Charmonium Physics*, Acta Physica Polonica proceedings B Vol. 1, (2008), supplement no. 3.
- [57] H. Muramatsu, *Recent studies of Charmonium Decays at CLEO*, ECONFC070805: 14, (2007), arXiv:0711.1927v2 [hep-ex].
- [58] E. Eichten et al., *Quarkonia and their transitions*, Rev. Mod. Phys. 80, (2008) 1161.
- [59] T. Barnes, *Charmonium at BES and CLEO-c*, arXiv:hep-ph/0406327v1.
- [60] Stefan and Bee, *The J/Psi and the Charmonium Spectrum*, backreaction.blogspot.com, December 20, 2007, online available at <http://backreaction.blogspot.com/2007/12/jpsi-and-charmonium-spectrum.html>, accessed on April 14, 2008.
- [61] K. Königsmann, *Radiative decays in the ψ family*, Physics Reports 139, Issue 5, June 1986, Pages 243-291.
- [62] T. Barnes, *The XYZs of charmonium at BES*, Int. J. Mod. Phys. A 21, (2006) 5583-5591, arXiv:hep-ph/0608103v1.
- [63] K. Gottfried, *Hadronic Transitions between Quark-Antiquark Bound States*, Phys. Rev. Lett. 40, (1978) 598.

- [64] C. -Z. Yuan (for the BES Collaboration), *Recent BES Results on Charmonium Decays*, arXiv:0711.4893v1 [hep-ex].
- [65] J. Z. Bai, et al., *Measurements of the Cross Section for $e^+e^- \rightarrow$ Hadrons, at Center-of-Mass Energies from 2 to 5 GeV*, Phys. Rev. Lett. 88, (2002) 101802. BES Collaboration.
- [66] Z. Li, et al., *Measurement of the branching fractions for $J/\psi \rightarrow l^+l^-$* , Phys. Rev. D 71, (2005) 111103. CLEO Collaboration.
- [67] J. Bolz and P. Kroll, *Exclusive J/ψ and ψ' decays into baryon-antibaryon pairs*, Eur. Phys. J. C 2, (1998) 545-556.
- [68] S. J. Brodsky and G. P. Lepage, *Helicity selection rules and tests of gluon spin in exclusive quantum-chromodynamic processes*, Phys. Rev. D 24, (1981) 2848.
- [69] V. L. Chernyak, A. A. Ogloblin and I. R. Zhitnitsky, Z. Phys. C 42, 583 (1989)
- [70] N. G. Stefanis and M. Bergmann, *Nucleon distribution amplitude: The heterotic solution*, Phys. Rev. D 47, (1993) 3685.
- [71] N. G. Stefanis and M. Bergmann, *Analysis of $\Delta^{++}(1232)$ isobar observables with improved quark distribution amplitudes*, Phys. Lett. B 304, (1994) 24.
- [72] T. Appelquist and H. D. Politzer, *Heavy Quarks and e^+e^- Annihilation*, Phys. Rev. Lett. 34, (1975) 43.
- [73] J. Z. Bai et al., *Measurement of $\psi(2S)$ decays to baryon pairs*, Phys. Rev. D 63, (2001) 032002. BES Collaboration.

- [74] M. Ablikim et al., *Measurements of $\psi(2S)$ decays to octet baryonantibaryon pairs*, Phys. Lett. B 648, (2007) 149155. BES Collaboration.
- [75] T. K. Pedlar et al., *Branching-fraction measurements of $\psi(2S)$ decay to baryon-antibaryon final states*, Phys. Rev. D 72, (2005) 051108. CLEO Collaboration.
- [76] O. Kamaev, *Rare Nonleptonic Decays of the Omega Hyperon: Measurements of the Branching Ratios for $\Omega^\mp \rightarrow \Xi_{1530}^{*0} \overline{(\Xi_{1530}^{*0})} \pi^\mp$ and $\Omega^\mp \rightarrow \Xi^\mp \pi^\pm \pi^\mp$* , PhD Thesis, Graduate College of the Illinois Institute of Technology, Chicago, Illinois, USA, December 2007.
- [77] G. Ramalho, K. Tsushima and F. Gross, *Relativistic quark model for the Ω^- electromagnetic form factors*, Phys. Rev. D 80, (2009) 033004.
- [78] D. Wu and J. L. Rosner, *Constituent quark description of nonleptonic hyperon decays*, Phys. Rev. D 33, (1986) 1367.
- [79] He, X. G., and G. Valencia. *$\Delta(I) = 3/2$ and $\Delta(S) = 2$ hyperon decays in chiral perturbation theory*, Phys. Lett. B 409, (1997) 469-473.
- [80] C. G. White et al., *Search for $\Delta(S) = 2$ non-leptonic hyperon decays*, Phys. Rev. Lett. 94, (2005) 101804. HyperCP Collaboration.
- [81] R. A. Briere et al. (CESR-c Taskforce, CLEO-c Taskforce, and CLEO-c Collaboration), Report No. CLNS 01/1742, 2001.
- [82] Draft paper, *First Evidence of $\psi(2S) \rightarrow \Omega^- \bar{\Omega}^+$* , submitted to BES Collaboration (<http://bes.ihep.ac.cn>, restricted access)

- [83] BESII Analysis memo, *First Evidence of $\psi(2S) \rightarrow \Omega^-\bar{\Omega}^+$* ,
(<http://bes.ihep.ac.cn>, restricted access)
- [84] G. R. Farrar and R. D. Jackson, Phys. Rev. Lett. 35, 1416 (1975); B. L. Ioffe, Phys. Lett. 63B, 425 (1976); A. I. Vainshtein and V. I. Zakharov, Phys. Lett. B 72, 368 (1978); S. J. Brodsky and G. P. Lepage, Phys. Rev. D 24, 2848 (1981).
- [85] R. -G. Ping and C. -Y. Pang, *Monte Carlo Generators for Tau-Charm-Physics at BESIII*, http://bes.ihep.ac.cn/bes3/phy_book/book/phy/generators_ping.pdf
- [86] B. Andersson, G. Gustafsson, and C. Peterson, *A semi-classical model for quark jet fragmentation*, Z. Phys. C 1 (12), 105116, 179.
- [87] J. C. Chen et al., *Event generator for $J\psi$ and $\psi(2S)$ decay*, Phys. Rev. D 62, (2003) 034003.
- [88] Yong-Sheng Zhu , High Energy Phys. Nucl. Phys. 30: 331-334, 2006
- [89] J. Filaseta, *Data Analysis for University Physics*, www.nku.edu, Last updated on March 31, 2004, online available at <http://www.nku.edu/filaseta/DataAnalysis.pdf>, accessed on May 31, 2008.
- [90] A. Ferrari et al., *An improved multiple scattering model for charged particle transport*, Nucl. Instr. Meth. B 71, (1992) 412.

- [91] C. Zeitnitz and T.A. Gabriel, *The GEANT-CALOR interface and benchmark calculations of ZEUS test calorimeters*, Nucl. Instr. and Meth. A 349, (1994) 106.